Revisiting the high tropospheric ozone over Southern Africa: role of biomass burning and anthropogenic emissions

Yufen Wang[1], Ke Li[1*], Xi Chen[1], Zhenjiang Yang[1], Minglong Tang[1], Pascoal M.D. Campos[2], Yang Yang[1], Xu Yue[1], and Hong Liao[1]

[1]Jiangsu Key Laboratory of Atmospheric Environment Monitoring and Pollution Control, Jiangsu Collaborative Innovation Centre of Atmospheric Environment and Equipment Technology, Joint International Research Laboratory of Climate and Environment Change, State Key Laboratory of Climate System Prediction and Risk Management, School of Environmental Science and Engineering, Nanjing University of Information Science and Technology, Nanjing, China
[2]CNIC-Centro Nacional de Investigação Científica, Ministério Do Ensino Superior Ciência, Tecnologia e Inovação, Avenida Ho Chi Minh N° 201, Luanda, Angola

*Correspondence to: keli@nuist.edu.cn

Abstract. Tropospheric ozone over Southern Africa is particularly high and causes tremendous health risks and crop yield losses. It has been previously attributed to the influence by biomass burning (BB), with a neglected contribution from anthropogenic emissions. However, due to the lack of measurements for ozone and its precursors, the modeled impacts of BB and anthropogenic emissions on tropospheric ozone were not well evaluated in Southern Africa. In this study, we combined the nested GEOS-Chem simulation with a horizontal resolution of $0.5° × 0.625°$ with available multiple observations at the surface and from space to quantify tropospheric ozone and its main drivers in Southern Africa. Firstly, BB emissions from current different inventories exhibit similar peaks in summer season but also have large uncertainties in Southern Africa (e.g., uncertainty of a factor of 2-3 in emitted NO_x). The model-satellite comparison in fire season (July-August) in 2019 shows that using the widely-used Global Fire Emissions Database Version 4.1 (GFED4.1) inventory, the model tends to overestimate by 87% compared to OMI NO_2, while the Quick Fire Emissions Database (QFED2) inventory can greatly reduce this model bias to only 34%. Consequently, the modeled tropospheric column ozone (TCO) bias was reduced from 14% by GFED4.1 to 2.3% by QFED2. In addition, the QFED2 also has a much better spatial representativeness than GFED4.1. The simulated surface daily maximum 8-hour mean (MDA8) ozone was decreased from 74 ppb by GFED4.1 to only 56 ppb by QFED2. This suggests a highly overestimated role of BB emissions in surface ozone if GFED4.1 is adopted. The model-observation comparison at the surface shows that the global Community Emissions Data System (CEDSv2) anthropogenic inventory tends to underestimate anthropogenic NO_x emissions in typical Southern African cities and likely misrepresented anthropogenic sources in some areas. That means that urban ozone and $PM_{2.5}$ concentrations in Southern Africa may be strongly underestimated. For example, a ten-fold increase in anthropogenic NO_x emissions can change ozone chemistry regime and increase $PM_{2.5}$ by up to 50 µg m^{-3} at the Luanda city. Furthermore, we also find that the newly TROPOMI can already capture the urban NO_2 column hotspots over low-emission regions like

1

34   Southern Africa while this is unavailable from the OMI instrument, highlighting the critical role of high-resolution
35   measurements in understanding atmospheric chemistry issues over Southern Africa. Our study presents a deeper
36   understanding of the key emission sources and their impacts over Southern Africa that will be helpful not only to formulate
37   targeted pollution controls, but also to enhance the capability in predicting future air quality and climate change, which
38   would be beneficial for achieving a healthy, climate-friendly, and resilient development in Africa.
39
40   **Keywords:** biomass burning, tropospheric ozone, Southern Africa, urban emissions

41   **1 Introduction**

42   Tropospheric ozone (O_3) is an important trace gas in the atmosphere, posing multifaceted threatens to public health, crop
43   yield, and global environment (Xu et al., 2018; Bourgeois et al., 2021). Complex photochemical reactions of nitrogen
44   oxides (NO_x = NO + NO_2) and volatile organic compounds (VOCs) in the presence of sunlight is the main source of
45   tropospheric ozone (Wang et al., 2022). These two ozone precursors are emitted from both anthropogenic and natural
46   sources. Great efforts have been made to reduce anthropogenic emissions, but ozone pollution is still challenging in many
47   urban regions across the globe (Gaudel et al., 2020; Lyu et al., 2023). Globally, it was estimated that ~365,000 premature
48   deaths could be attributed to ozone pollution in 2019 (Murray et al., 2020). The urban population exposed to ozone was
49   increased at a trend of 0.8% per year from 2000 to 2019, and the largest increases of daily maximum 8-hour mean (MDA8)
50   ozone occurred in Africa and India (Sicard et al., 2023). However, due to the lack of comprehensive studies on
51   tropospheric ozone pollution in Southern Africa, it is urgent to explore the major source contributions driving ozone
52   pollution over these less-studied regions. A better understanding of the major emission sources is not only helpful to
53   formulate actionable targeted pollution controls and to reduce air pollution risks, but also important to predict future air
54   quality in developing regions under the rapid changing of emissions and climate change.
55
56   Biomass burning (BB) emits large amounts of air pollutants that are important ozone precursors (Qin et al., 2024). Africa
57   is frequently exposed to intense BB (Vernooij et al., 2021), contributing to 70% of the global BB area and nearly 75% of
58   global infant deaths attributed to BB pollutants (Jiang et al., 2020; Hickman et al., 2021). Exposure to air pollution from
59   BB has strong differences in socioeconomic levels (Yue et al., 2024), with the most heavily exposed populations being in
60   Southern Africa (Xu et al., 2023). Due to the complex climate types and unique lifestyles, BB in Africa during June-August
61   months is concentrated over Southern Africa (Meyer-Arnek et al., 2005; Williams et al., 2010), and this "slash-and-burn"
62   agricultural activity could lead to the very high ozone concentrations over Southern Africa. As shown in **Figure S1**, surface
63   ozone concentrations in Southern Africa were simulated exceeding 100 ppb in July, making it to be the highest ozone level
64   worldwide. This is consistent with the previous modeling findings that BB activities are the dominant driver of tropospheric

ozone in this region (V. Clarmann et al., 2007). At the city level, Rwanda with observed daily ozone maximum of 70 ppb during the dry season (Dewitt et al., 2019) can be affected by the transport of BB from Northern and Southern Africa. The high ozone is mainly driven by BB NO_x emissions; for example, the Southern African BB can increase NO_x concentrations by a factor of 2-5 in July-August months (Hoelzemann, 2006). Although BB has a great impact on ozone and its precursors in Southern Africa, there are few quantitative studies on this issue.

The popular way of quantifying the role of BB is to conduct chemical transport modeling, e.g., using the ECHAM5-MOZ (Aghedo et al., 2007), GEOS-Chem (Wang et al., 2022; Marvin et al., 2021), and WRF-Chem (Yang et al., 2022). The ECHAM5-MOZ model simulations show that BB can increase surface ozone by more than 50 ppb in Central Africa in June-August during 1997-2001 (Aghedo et al., 2007). Williams et al. (2010) used the Tracer Model version 4 to simulate June-August air pollution in 2006, and they showed that BB in Southern Africa is the largest source of carbon monoxide and ozone precursor emissions in Africa. However, model assessment is highly dependent on BB emission inventories and there is a lack of comparative studies of different BB inventories over the Southern Africa. This is because existing BB emission inventories have large uncertainties in Africa (Petrenko et al., 2012; Shi et al., 2015). The most widely-used inventory for global model simulations is the Global Fire Emissions Database (GFED) (Shi et al., 2020), and other BB inventories include the Quick Fire Emissions Database (QFED), the Global Fire Assimilation System (GFAS), and the Fire Inventory from NCAR (FINN). The uncertainties of a factor of 2-10 among these inventories source from estimated burned area, emission factors, and vegetation type (Fu et al., 2022). Depending on how fire emissions are calculated, these inventories can be divided into two categories: the fuel-based bottom-up estimation (e.g., GFED and FINN) (Pechony et al., 2013; Nikonovas et al., 2017) and the satellite-derived top-down estimation (e.g., QFED and GFAS) (Nikonovas et al., 2017). In addition, the injected height of BB emissions is also a key factor in determining the residence time of pollutants in the atmosphere that would impact the spatiotemporal distribution of tropospheric ozone (Rémy et al., 2017). Therefore, it is urgent to take advantage of observational constraints to evaluate the current BB inventories and quantify their impacts on tropospheric ozone in Africa.

In addition to the effects of BB, tropospheric ozone can be also affected by anthropogenic emissions in Africa. Although the intensity of anthropogenic emissions is relatively low in Africa, its impact at the urban scale cannot be ignored. With the rapid urbanization (Liousse et al., 2014), mean concentrations of surface SO_2, $PM_{2.5}$, and PM_{10} in Luanda have exceeded European Union human health protection limits (Campos et al., 2021). More importantly, anthropogenic emissions (e.g., black carbon) are projected to be comparable with BB emissions by 2030 in Africa (Liousse et al., 2014). Projection studies also pointed out that 50% of the population will be expected to live in cities by 2050 (Aucoin and Bello-Schünemann, 2016), resulting in a significant increase in the population exposure to ozone in Africa. With air pollution becoming a major

97   cause of premature deaths in Africa (Julien et al., 2018), urban air pollution will likely pose more challenges in the context

98   of increasing anthropogenic emissions (Roy, 2016; Marais and Wiedinmyer, 2016; Zhang et al., 2021). However, whether

99   the current anthropogenic emission inventories are reasonable in urban Southern Africa remains unclear.

100

101   Lack of surface observations is a major challenge for assessment of emission inventories in Africa. About 66% of African

102   countries do not have regular air quality monitoring (Fajersztajn et al., 2014), particularly few in Southern Africa (Julien

103   et al., 2018). Recently, there are continuous surface measurements available at several major cities over Southern Africa

104   (**Figure 1**), together with the high-resolution satellite observations (e.g., TROPOMI), which could be very helpful to detect

105   urban air pollution in this region. With the worsening air pollution in Africa (Sicard et al., 2023), it is particularly timely

106   to take advantage of these valuable measurements to assess the key drivers of high tropospheric ozone in Southern Africa.

107

108   As abovementioned, there are notable uncertainties in the estimation of major emission sources over Southern Africa.

109   Assessing and predicting the impacts of emissions on air quality and health risks rely heavily on model simulations, and

110   these uncertainties in emission inventories can affect the development of effective control strategies. We therefore need to

111   utilize surface and satellite observations to gain a comprehensive understanding of the emission source contributions in

112   Southern Africa. This will help to develop effective mitigation measures to realize the Sustainable Development Goals for

113   having a healthy, climate-friendly, and resilient development in Africa.

114

115   Here we integrated the high-resolution GEOS-Chem model and newly-available measurements to estimate the impact of

116   biomass burning and anthropogenic emissions on tropospheric ozone over Southern Africa. The aim of this study is: 1) to

117   quantify the role of BB emissions on regional tropospheric ozone over Southern Africa, and 2) to assess the

118   representativeness of anthropogenic emission inventories in urban Southern Africa and their impacts on urban ozone

119   pollution. Observational data, model description and experimental setup are presented in Section 2. Section 3.1 shows the

120   major emission sources and the high tropospheric ozone issue over Southern Africa. The estimated impacts of biomass

121   burning and anthropogenic emissions on tropospheric ozone are analysed in Sections 3.2 and 3.3, respectively. Conclusions

122   and discussion are given in Section 4.
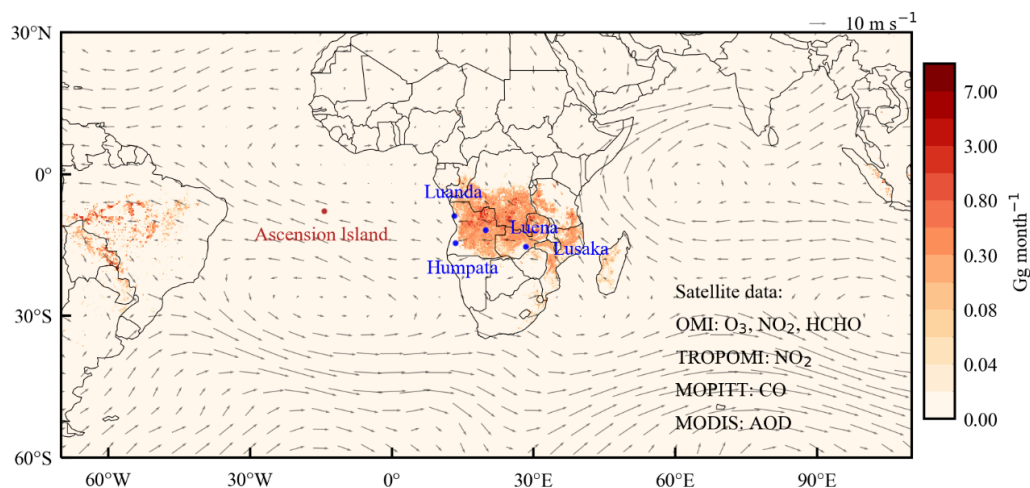
Figure 1. The biomass burning NO_x emissions (shaded) and 850hpa wind fields. The BB NO_x emissions are for July-August 2019 from the GFED4.1 inventory (unit: Gg month^{-1}). Blue dots represent the locations of surface observations and red dot denotes the ozonesonde measurement; and satellite data used in this study are listed in the lower right corner.

2 Measurement data and model description

2.1 Surface measurements

Figure 1 shows the locations of the four surface observation sites over Southern Africa. Hourly and daily real-time air quality indexes (AQI) for NO_2 and $PM_{2.5}$ were obtained from the Worldwide Air Quality Index (https://aqicn.org/station). The AQI can be converted to pollutant concentrations based on the website's AQI Calculator. These four sites record continuous measurement data in the study area, namely: Humpata in Angola (14°95'S, 13°44'E), Luanda in Angola (8°80'S, 13°23'E), Luena in Angola (11°76'S, 19°91'E), and Lusaka in Zambia (15°41'S, 28°29'E). The stations in Angola and Zambia have been operating since mid-May 2023 and February 2022, respectively, and data for June-August 2023 were selected for this study. To evaluate modeled ozone profiles, we adopted the Ascension Island's ozonesonde data from the Southern Hemisphere Additional Ozone Sounding (SHADOWZ) network, which measured ozone profile from 1998 (Thompson et al., 2000).

2.2 Satellite data

In order to investigate the model results driven by different BB emission inventories and the anthropogenic emission inventories, multiple observations from the OMI (https://disc.gsfc.nasa.gov/datasets/), TROPOMI (https://www.earthdata.nasa.gov/sensors/tropomi), MODIS (https://ladsweb.modaps.eosdis.nasa.gov/search/), and MOPITT (https://giovanni.gsfc.nasa.gov/giovanni/) satellite instruments were used (Table 1). The OMI sensor observes

143 the globe once a day and is capable of obtaining the column concentration distributions of a variety of tropospheric trace
144 gases (e.g., NO_2 and O_3). The TROPOMI sensor is a troposphere-specific observational instrument, and Wang et al. (2020)
145 have compared the NO_2 concentrations of OMI and TROPOMI with observations. As for MODIS AOD, Shi et al. (2019)
146 compared observations from 400 stations of the Aerosol Robotics Network (AERONET) with the MODIS AOD, and
147 demonstrated that the MODIS was able to better capture the spatial and temporal variations of AERONET AOD (Zhang et
148 al. 2024). MOPITT was launched in December 1999 on board the Earth observation satellite Terra with a 10:30 am equator
149 crossing time (Kopacz et al., 2010). Here, as listed in **Table 1**, we used tropospheric ozone, NO_2, and HCHO observations
150 from OMI with resolutions of $1° \times 1.25°$, $0.25° \times 0.25°$, and $0.05° \times 0.05°$, respectively, as well as NO_2 observations from
151 TROPOMI with a resolution of $0.125° \times 0.125°$. AOD and CO observations with a resolution of $1° \times 1°$ are from MODIS
152 and MOPITT, respectively. We sampled the model simulation results consistent with satellite overpass times in the
153 following comparisons. Although these satellite datasets have been well employed to reflect emission changes, their
154 uncertainties are also notable due to biases in slant column density, air mass factor, and stratosphere-troposphere separation.
155 For example, the reported uncertainties in NO_2 columns from OMI and TROPOMI are 25-50% and they can be increased
156 to 50-100% in terms of OMI HCHO columns.

157 **Table 1**. Satellite and surface observations used for this study.

Species		Spatial resolution/ Site locations	Time
O_3	OMI	$1° \times 1.25°$	July-August 2019
NO_2	OMI	$0.25° \times 0.25°$	2019-2020
HCHO	OMI	$0.05° \times 0.05°$	July-August 2019
NO_2	TROPOMI	$0.125° \times 0.125°$	2018-2023
AOD	MODIS	$1° \times 1°$	July-August 2019
CO	MOPITT	$1° \times 1°$	July 2019
$PM_{2.5}$	Humpata	(14°95' S, 13°44' E)	June-August 2023
	Luanda	(8°80' S, 13°23' E)	
	Luena	(11°76' S, 19°91' E)	
	Lusaka	(15°41' S, 28°29' E)	
NO_2	Humpata	(14°95' S, 13°44' E)	June-August 2023
	Luanda	(8°80' S, 13°23' E)	
	Luena	(11°76' S, 19°91' E)	
O_3	Ascension Island	(7.56 S, 14.22 E)	July-August 2017-2019

158

159 **2.3 Biomass burning emission inventories**

160 In this study, six BB emission inventories were compared: GFED4.1, GFED5, GFAS, QFED2, FINNv1.5, and FINNv2.5.
161 The GFED4.1 inventory provides dry matter emissions based on the area of BB and vegetation types from MODIS
162 observations (Marvin et al., 2021; Zhang et al., 2018). The GFED5 is an updated version of GFED4.1 and the GFED5
163 global burned area is 61 % higher than GFED4.1 (Chen et al., 2023). The GFAS inventory estimates the amount of dry
164 matter burning based on fire radiative power (FRP) (Vongruang et al., 2017). The QFED2 inventory is based on the FRP
165 method and draws on the cloud correction method developed in GFAS with the high spatiotemporal resolution. FINNv1.5
166 calculates dry matter combustion using fire hot spots (FHS) data to calculate the burned area, and FINNv2.5 builds on this
167 with extensive updates to the burned area, vegetation types, and chemicals emitted. In particular, FINNv2.5 adopted the
168 active fire detections from the Visible Infrared Imaging Radiation Suite (VIIRS) to better capture small fires, and used
169 multiple satellite products for daily fire emissions estimates (i.e., MODIS + VIIRS fire detections). The estimated BB NO_x
170 emissions from these inventories will be further discussed in Section 3.2.1.

171 **2.4 GEOS-Chem Model**

172 The atmospheric composition in Africa was simulated by using the nested version of the three-dimensional global chemical
173 transport model (GEOS-Chem, version 13.3.3; http://acmg.seas.harvard.edu/geos/), which was driven by the Modern-
174 Era Retrospective analysis for Research and Applications version 2 (MERRA-2) meteorological reanalysis dataset. The
175 model domain was for Africa (35°S - 30°N, 17°W - 50°E) with a horizontal resolution of 0.5° × 0.625° and a vertical
176 configuration of 47 layers. The chemical boundary conditions for the nested simulation are provided by the global GEOS-
177 Chem simulation with a horizontal resolution of 2° × 2.5°, which was updated every three hours. GEOS-Chem model
178 includes fully coupled ozone-NO_x-hydrocarbon-aerosols chemistry mechanisms. $PM_{2.5}$ components include sulfate, nitrate,
179 ammonium, dust, sea salt, organic carbon (OC), and black carbon (BC) (Park et al., 2004).

180

181 In Africa, anthropogenic emissions are from the Community Emissions Data System (CEDS) (Hoesly et al., 2018) and
182 biogenic emissions are from the Model of Emissions of Gases and Aerosols from Nature (MEGAN) version 2.1 (Guenther
183 et al., 2012). We simulated hourly concentrations of ozone, NO_2, and other pollutants in Africa using the nested GEOS-
184 Chem model with a set of sensitivity simulations (**Table 2**). Here we focused our experiments on July-August 2019 for all
185 sensitivity and benchmark simulations. In order to investigate the effect of BB on tropospheric ozone, we conducted three
186 model experiments. Firstly, we used GFED4.1 and QFED2 inventories to simulate the hourly air pollutant concentrations
187 for July-August, 2019 (Run_GFED and Run_QFED), respectively, and validated the model results with satellite
188 observations. Then, we conducted a sensitivity experiment by scaling down the QFED NO_x emissions to be consistent with

189   satellite NO$_2$ observation (Run_QFED_66%NO$_x$). We used two different BB inventories and turned off aerosol chemistry

190   to explore the effect of aerosols on ozone (Run_GFED_no-aerosol and Run_QFED_no-aerosol). We also explored the

191   effect of emission height on simulated tropospheric ozone by emitting BB pollutants only within the PBL

192   (Run_QFED_PBL).

193

194   After evaluating the BB emission inventories at the regional scale, we set up a series of experiments to explore the impact

195   of anthropogenic emissions on tropospheric ozone in Southern Africa. Considering that surface air pollutant measurements

196   are only available for June-August 2023, and then we used the up-to-date QFED inventory to simulate concentrations of

197   NO$_2$ and PM$_{2.5}$ in June-August 2023 (Run_QFED_2023) and compared them with five surface air quality observations.

198   We also conducted model simulations for January-February 2020 (Run_QFED_2020) to explore the effect of

199   anthropogenic emissions on tropospheric ozone during the non-fire season. It is noted that we fixed the anthropogenic

200   emissions from CEDS at 2019 in all these simulations due to the lack of up-to-date anthropogenic emission data. Based on

201   the underestimation of surface NO$_2$ observations in the model, we explored the sensitivity of ozone and PM$_{2.5}$

202   concentrations to anthropogenic NO$_x$ changes by a factor of 10 or 20 over the Southern Africa (Run_QFED_Anth10NO$_x$

203   and Run_QFED_Anth20NO$_x$); at the city scale, we explored the effects of perturbing anthropogenic NO$_x$ emissions in

204   Luanda by a factor of ten for difference sectors (i.e., power plant, industrial, and transportation) (Run_QFED_Anth_10NO$_x$

205   _Sector).

206

207   Finally, we conducted two set of sensitivity simulations to attribute ozone to different emission sources, by turning off BB

208   emissions, natural emissions (i.e., biogenic VOC and soil NO$_x$), and anthropogenic emissions, respectively (Table 1). In

209   particular, we compared the ozone source attribution between the simulations by using the CEDS inventory and 10-fold

210   CEDS NO$_x$ emission.

211 **Table 2**. GEOS-Chem model simulations

	Experiments	BB emissions	Anthropogenic emissions
Impacts of biomass burning (July-August 2017-2019）	Run_GFED	GFED4.1	CEDSv2
	Run_QFED	QFED2	CEDSv2
	Run_QFED_66%NO$_x$	34% reduction in QFED2 NO$_x$ emissions	
	Run_GFED_no-aerosol	Aerosol chemistry was turned off	
	Run_QFED_no-aerosol		
	Run_QFED_PBL	100% emissions below the PBL*	
Impacts of anthropogenic emissions	Run_QFED_2023		CEDSv2
	Run_QFED_Anth10NO$_x$	QFED2 June-August 2023	10-fold NO$_x$ emissions
	Run_QFED_Anth20NO$_x$		20-fold NO$_x$ emissions
	Run_QFED_Anth_10NO$_x$_Sector		10-fold NO$_x$ emissions of energy, industry, and transportation sectors, respectively
	Run_QFED_2020	QFED2 January-February 2020	CEDSv2
Ozone source attribution （July-August 2019）	Run_QFED_noBB	BB emissions were turned off	
	Run_QFED_noNatl	BVOC and soil NO$_x$ emissions were turned off	
	Run_QFED_noAnth	Anthropogenic emissions were turned off	
	Run_QFED_Anth10NO$_x$_noBB	BB emissions were turned off	
	Run_QFED_Anth10NO$_x$_noNatl	BVOC and soil NO$_x$ emissions were turned off	
	Run_QFED_Anth10NO$_x$_noAnth	Anthropogenic emissions were turned off	

212 *The baseline simulation follows the vertical distribution of QFED2 emission (i.e., 65% emissions below the PBL and 35%
213 emissions into the free atmosphere).

3. Results and discussion

3.1 Emission sources and simulated high ozone over Southern Africa
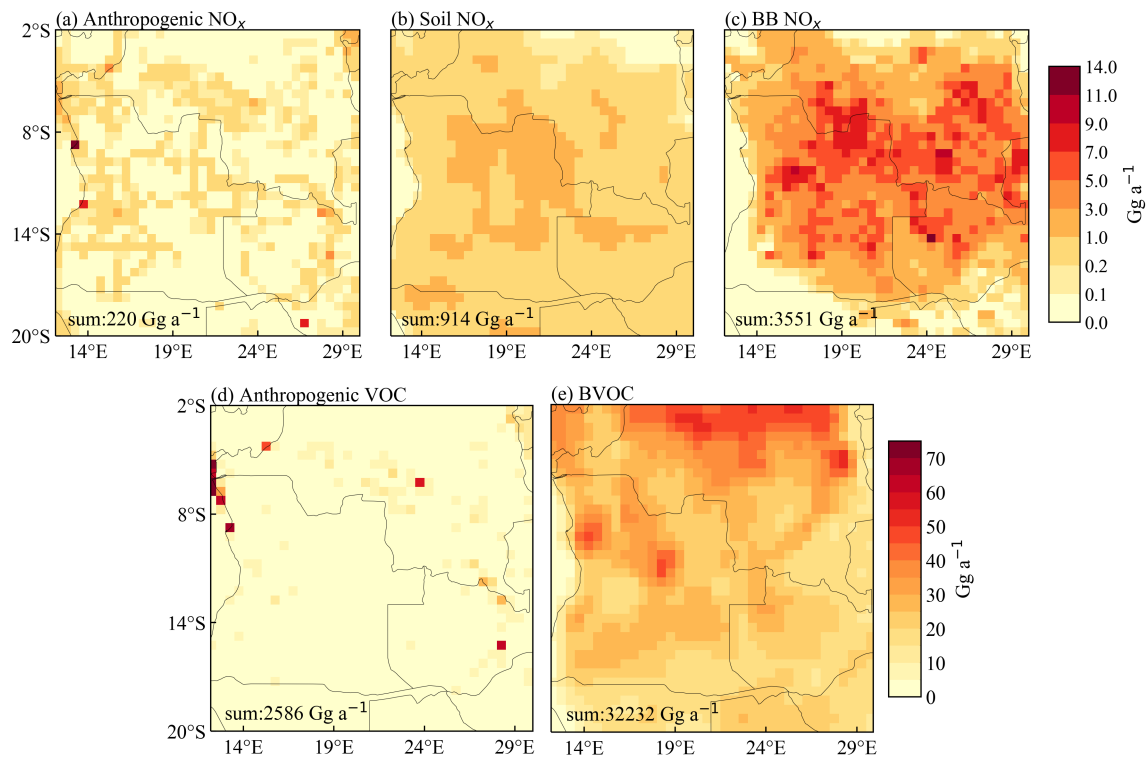
Figure 2. Spatial distributions of annual emissions of anthropogenic NO_x, soil NO_x, biomass burning NO_x, anthropogenic VOC, and BVOC in 2019 (unit: Gg a^{-1}). Anthropogenic NO_x and VOC are from CEDSv2 inventory, soil NO_x and BVOC are calculated by the GEOS-Chem model, and biomass burning NO_x and VOC are from GFED4.1 and QFED2 inventory.

We compared the annual emissions of anthropogenic NO_x, soil NO_x, BB NO_x, as well as anthropogenic VOCs (AVOC) and biogenic VOCs (BVOC) over Southern Africa in 2019, as presented in **Figure 2**, which were estimated at 220 Gg a^{-1}, 914 Gg a^{-1}, 3551 Gg a^{-1}, 2586 Gg a^{-1}, and 32,232 Gg a^{-1}, respectively. It should be noted that here BB NO_x emissions are from the GFED4.1 inventory. In terms of NO_x emissions, BB emission is the largest contributor and is about 16 times of NO_x emissions from anthropogenic sources. The regions with high anthropogenic emissions are mainly Luanda, Kinshasa, and Lusaka which are the capitals of Angola, the Democratic Republic of the Congo (DRC), and Zambia, respectively. High vegetation cover in Southern African region leads to high BVOC emissions which are about 12 times of AVOC emissions.

229 Seasonally, **Figure 3** presents the monthly variations of ozone precursor emissions averaged over Southern Africa in 2019.

230 The BVOC emission exhibits a strong seasonal pattern ranging from 2000 Gg month^{-1} to 4000 Gg month^{-1}, and it peaks in

231 March and then decreases to the minimum in July-August. This seasonality is consistent with the seasonal variation in

232 isoprene emissions in Southern Africa in 2006 as reported by Williams et al. (2009). We can also see that NO$_x$ from BB

233 peaks during June-August, which is consistent with the results of Boschetti and Roy (2008). Emissions of BB NO$_x$ in

234 January-April and November-December were relatively small. BB VOC has similar seasonal variability in both inventories,

235 but the GFED4.1 inventory emits 2-3 times as much as the QFED2 inventory in fire season. The BVOC emissions are

236 generally higher than BB VOC emissions except for those in July-August months from the GFED4.1 inventory. The

237 seasonal contrast in BB NO$_x$ and BVOC emissions highlights the importance of BB in the production of high summer

238 tropospheric ozone in this region (Vieira et al., 2023).

239
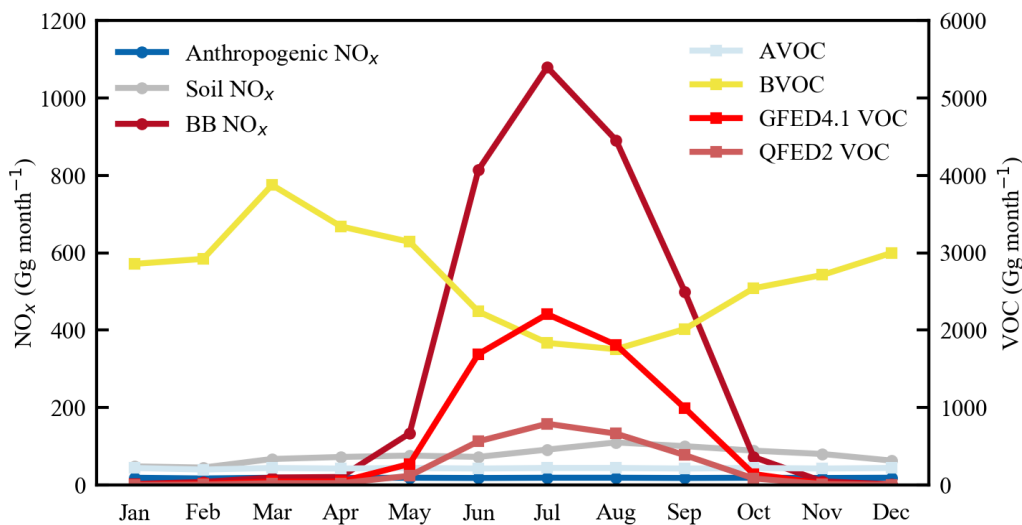
240 **Figure 3.** Seasonal variations in anthropogenic NO$_x$ (deep blue), soil NO$_x$ (grey), biomass burning NO$_x$ (red), biomass

241 burning VOC (red), anthropogenic VOC (blue), and biogenic VOC (yellow) emissions in 2019 (unit: Gg month^{-1}).

242 Anthropogenic NO$_x$ and VOC are from CEDSv2 inventory, soil NO$_x$ and BVOC are calculated by the GEOS-Chem model,

243 and biomass burning NO$_x$ and VOC are from GFED4.1 and QFED2 inventory.

244

245 Simulated spatial distribution of MDA8 ozone in Africa from July to August 2019 obtained by using the GEOS-Chem

246 model and the GFED4.1 inventory (Run_GFED) as in **Figure 4a**. The regional average of MDA8 ozone in Southern Africa

247 is about 74 ppb and the maximum can be up to 120 ppb in northern Angola and southwest Congo. Dewitt et al. (2019)

248 observed a daily ozone maximum of 70 ppb during the dry season in Rwanda, which is adjacent to the DRC, in 2015-2017.
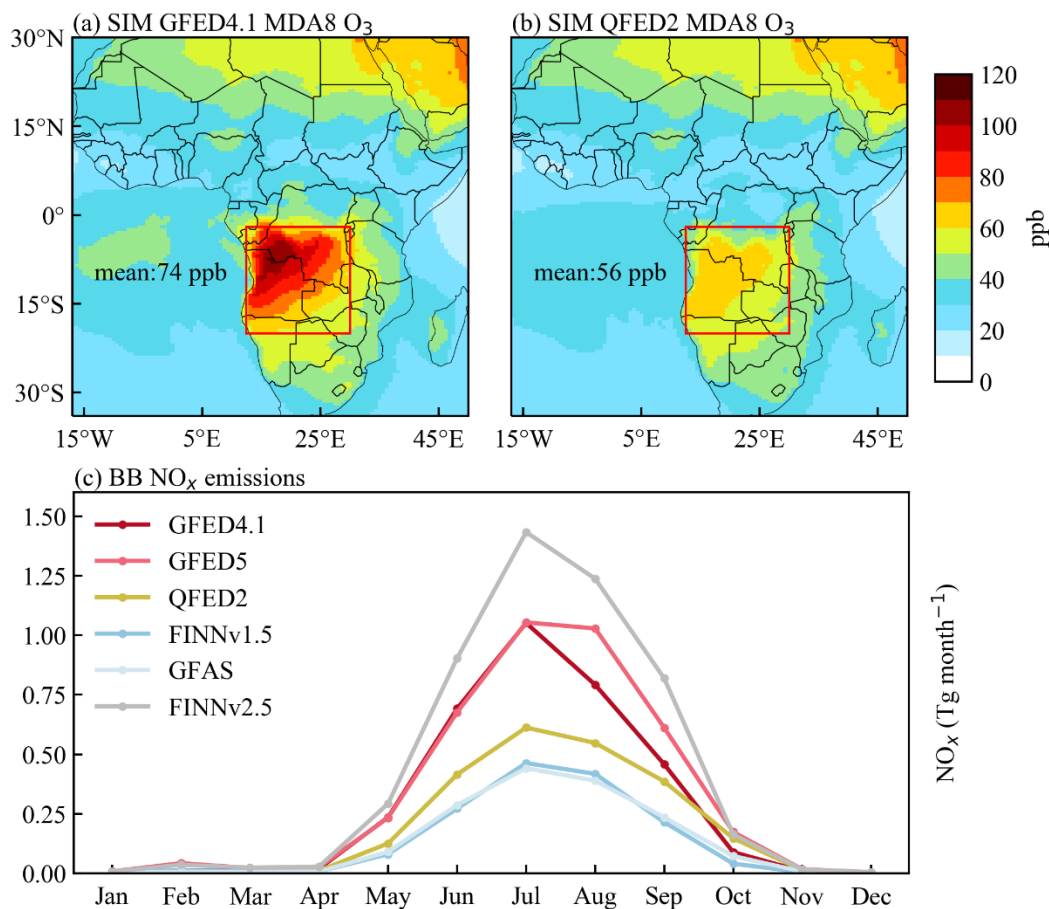
Figure 4. Differences in BB NO_x emissions and modeled surface ozone from different inventories. (a-b) Surface MDA8 ozone simulated by GEOS-Chem model for July-August 2019 by the GFED4.1 and QFED2 inventories, respectively. (c) Monthly BB NO_x emissions in 2014 averaged over the Southern African region.

Based on our simulation results, it can be found that the daily maximum ozone during the BB season is 86 ppb for Rwanda in the Run_GFED run, compared to only 62 ppb in Run_QFED run. Compared to the observed ozone in Rwanda, it may indicate an overestimation in the baseline simulation (Run_GFED). **Figure 5a** shows the spatial distribution of simulated tropospheric column ozone concentrations (TCO), with maximum values of up to 50 DU mainly in northern Angola and southwest Congo. Higher TCO levels are also seen over the Atlantic Ocean, which are mainly associated with long-range transport (Williams et al., 2010; Meyer-Arnek et al., 2005). Also, in Figure S2, we find that the GEOS-Chem simulated (Run_QFED) and OMI tropospheric ozone columns are in good agreement over the Atlantic Ocean after

12
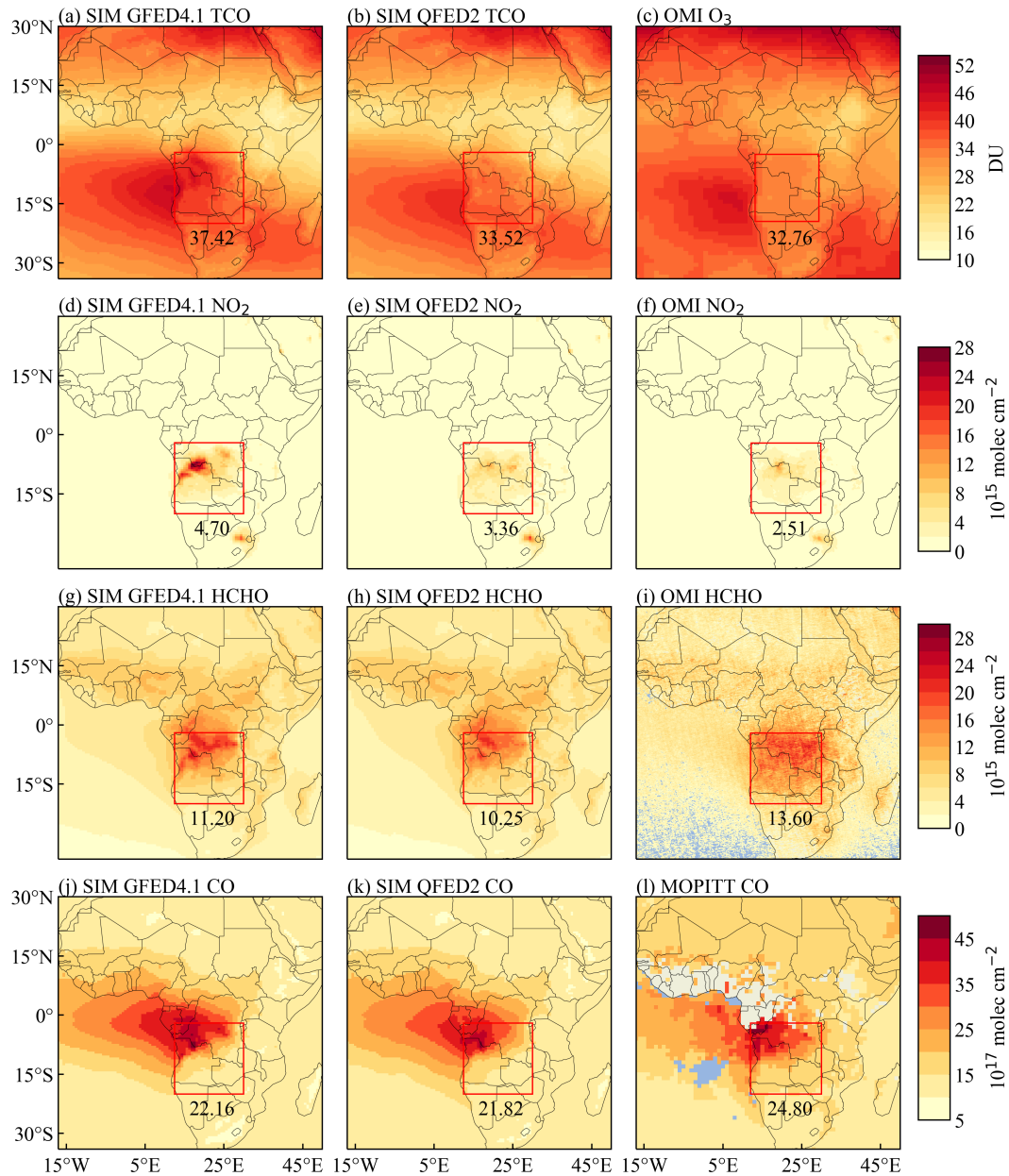
Figure 5. The comparison of GEOS-Chem simulated (left and middle panels) and satellite-based (right panels) tropospheric columns for ozone and its precursors. The simulated TCO, NO_2, HCHO, and CO columns in Africa for July-August 2019 were driven by the GFED4.1 and QFED2 inventories, respectively. For CO satellite data, only the July value was used due to the large amount of missing measurement in August. The numbers in the figure are the mean values in the red boxed area.

267 individually subtracting the background ozone values. Considering the strong seasonal variation of surface ozone in
268 Southern Africa (**Figure S3**) and the estimated ozone precursors from different sources in Figure 3, here the large
269 differences in simulated surface ozone with different BB inventories demonstrate that BB contributes greatly to high ozone
270 concentrations during the fire season in Southern Africa. As such, a better understanding of the high ozone over Southern
271 Africa would depend on the accurate estimate of BB emissions.

3.2 Impacts of biomass burning (BB) on tropospheric ozone

3.2.1 Uncertainties in BB emission inventories

274 Although the GEOS-Chem model has been widely employed for modeling tropospheric ozone globally (Balamurugan et
275 al., 2021; Li et al., 2023), its evaluation against measurements over Southern Africa is very limited. In order to accurately
276 evaluate the effects of BB emissions on tropospheric ozone, we need to take the uncertainties from different BB emissions
277 into account (Wiedinmyer et al., 2023).

279 We compared the monthly emissions of BB NO_x in 2014 for the Southern Africa from the six emission inventories
280 (GFED4.1, GFED5, QFED2, GFAS, FINNv1.5, and FINNv2.5), as illustrates in **Figure 4c**. All of the six BB inventories
281 share the similar seasonality in NO_x emissions, but there are large differences with a factor of 2-3 in estimated emission
282 intensities, particularly in the dry season. The inventory was divided into two groups based on the level of emissions, with
283 the high emission groups being FINNv2.5, GFED5, and GFED4.1. FINNv2.5 shows the highest BB NO_x emissions, which
284 are 45% higher than GFED4 emissions and 130% higher than QFED2 emissions, but Wiedinmyer et al. (2023) also suggests
285 that FINNv2.5 probably tends to overestimate NO_x emissions in Africa. GFED5 is an updated version from GFED4.1, and
286 their difference in NO_x emissions is minimum in January-July and enlarged in August. The low emission groups are:
287 QFED2, GFAS, and FINNv1.5. GFAS and FINNv1.5 resemble in the estimated NO_x emissions but both of them are
288 significantly lower than the other inventories. This lower estimate in the bottom-up FINNv1.5 inventory may be attributed
289 to the underestimated burned area and emissions (Wiedinmyer et al., 2011) , and the lower top-down GFAS estimate could
290 be due to a smaller emission factors (Liu et al., 2020). Therefore, in the following, we will use the GFED4.1 and QFED2
291 inventories to represent the high estimate and low estimate of BB NO_x emissions for Southern Africa, respectively.

293 Spatially, there are also evident differences among different biomass burning inventories (**Figure S4**). The spatial
294 distribution of the high values in GFED4.1 and QFED2 is generally consistent with a spatial correlation coefficient of 0.76,
295 both showing high emissions in northeastern Angola. In contrast, the GFED5 inventory has high NO_x emissions
296 concentrated in southwestern Congo, and its spatial distribution differs considerably with QFED2. The GFAS inventory
297 has a similar spatial distribution with QFED2 (a correlation coefficient of 0.84), but GFAS cannot capture the localized

298 high emissions as shown in QFED2 and GFED4.1. However, the FINNv1.5 and FINNv2.5 exhibit a very different spatial
299 distribution compared to other inventories, with low emissions in Angola and high emissions in the Congo region. Their
300 spatial correlation coefficients with the QFED2 inventory are 0.06 and 0.31, respectively.

302 In addition to NO_x emissions, the VOC emissions are the highest in GFED5 and FINNv2.5 inventories, and the other four
303 inventories show much smaller VOC emissions. Each inventory adopts different specific ratios for emitted chemical
304 species, but they also differ with each other. For example, there is a NO_x/OC ratio of 1:0.6 in GFED4.1, 1:1.5 in GFED5,
305 GFAS, and FINNv1.5, 1:3 in QFED2, and 1:1 in FINNv2.5 (**Figure S5**).

3.2.2 Simulated tropospheric ozone with different BB emissions

307 The simulated spatial distribution of MDA8 ozone in Africa during the fire season (July-August) in 2019 by using the
308 GEOS-Chem model with the GFED4.1 and the QFED2 inventories, respectively (**Figures 4a-4b**). The simulated surface
309 MDA8 ozone by the GFED4.1 inventory is 74 ppb over Southern Africa, which is 32% higher than the value of 56 ppb by
310 the QFED2 inventory. The maximum value of MDA8 ozone by the GFED4.1 inventory can reach up to 120 ppb, but the
311 maximum value by the QFED2 inventory is only 70 ppb. This remarkable discrepancy suggests that the uncertainties in
312 BB emissions could play an important role in simulating surface ozone over Southern Africa. This is consistent with
313 previous work that BB emissions lead to strong ozone increases in Southern Africa during the fire season (V. Clarmann et
314 al., 2007; Jaffe and Wigder, 2012). For the tropospheric ozone, **Figures 5a-5b** show the simulated spatial distribution of
315 TCO by using the GFED4.1 and QFED2 inventories. In contract to surface ozone, the regional average of TCO simulated
316 by the GFED4.1 inventory is only 4 DU (11%) higher than that simulated by the QFED2 inventory. We will show the
317 simulated ozone difference between these two inventories is mainly caused by BB NO_x emissions, while BB VOC
318 emissions only impact ozone levels slightly (**Figure S6**).

320 To evaluate the model performance in simulating the vertical profile of tropospheric ozone in Africa, we compared the
321 model results with ozonesonde observations from Ascension Island, UK (7°96'S, 14°91'W) in **Figure 6**. As shown in
322 **Figure 1**, Ascension Island is located downwind of the high BB area, and ozone and its precursors from BB can be
323 transported from Southern Africa to the South Atlantic (Mari et al., 2008), leading to ozone enhancement in Ascension
324 Island (Jenkins et al., 2021). The ozone concentrations modeled by GEOS-Chem respond well to the ozonesonde
325 observations in terms of vertical distribution, and in particular the model captures the variation in observations with altitude
326 well. The differences in ozone vertical distribution due to the two BB inventories are notable in the troposphere below 6
327 km, in particular at the altitude range of 3-6 km (**Figure S7**). Compared to the ozonesonde observations, this bias can be
328 also found while GEOS-Chem captures the vertical ozone variations well regardless of which inventory is used. This is

329   consistent with the results of small TCO differences in **Figures 5a-5b**. Compared to the ozonesonde observations, GEOS-

330   Chem captures the ozone variations well regardless of which inventory is used.

331

3.2.3 Satellite constraints on BB emission estimates

333   In order to evaluate the tropospheric ozone simulation in Africa region, in **Figure 5 and Table S1** we compared the

334   simulated columns with GFED4.1 and QFED2 inventories against satellite observations of TCO and ozone precursors (e.g.,

335   NO_2, CO, and HCHO). The simulated TCO with GFED4.1 inventory shows high values of up to 50 DU near the fire source

336   regions in northern Angola and southern DRC, and in the downwind region over Atlantic Ocean. The OMI TCO has the

337   regional average of 37.4 DU, suggesting an overestimation of 14% in the GFED4.1 simulation relative to OMI. In contrast,

338   the simulated TCO with QFED2 inventory is strongly spatially consistent with the OMI satellite, with a slight

339   overestimation of 2.3%.

340

341   We also compared the simulated and observed tropospheric NO_2 columns, illustrated in **Figures 5d-5e**. The GFED4.1

342   inventory simulation exhibits high value of up to 28×10^{15} molecule cm^{-2} near the BB source region, but there is a large

343   overestimation of 87% with respect to the OMI satellite data. Similar conclusions are also from Anderson et al. (2021) that

344   the model using the GFED4.1 inventory can capture high NO_2 in Africa but the bias was as high as 100%. This is in

345   agreement with previous studies that model simulations trend to produce a high bias towards BB activities in Africa (Souri

346   et al., 2024). However, the QFED2 inventory simulation can greatly reduce this high bias, with an overestimation of only

347   34%. In **Figure S8**, we also compared model results with the TROPOMI satellite, and a similar high bias was also found

348   in the modeled NO_2 columns. If we further have QFED2 NO_x emissions reduced by 34%, as shown in **Figure S9**, it can

349   effectively reduce the bias for NO_2 columns from 34% to 0.4% and reduce the overestimation of the TCO columns to 1.1%.

350   It is noted that this comparison between the simulated and satellite-based tropospheric columns could be biased due to their

351   different representativeness in vertical profiles of chemical species. Anyway, this sensitivity simulation demonstrates the

352   importance role of BB NO_x emissions in tropospheric ozone production. In contrast, we find that the BB VOC emissions

353   from GFED4.1 inventory are about 3 times the QFED2 inventory in fire season, but the regional mean changes are only

354   2.5 ppb for MDA8 ozone and 0.94 DU for TCO for July-August 2019 in response to a tripled QFED2 VOC emissions

355   (**Figure S6**).

Ascension Island, July-August 2017-2019
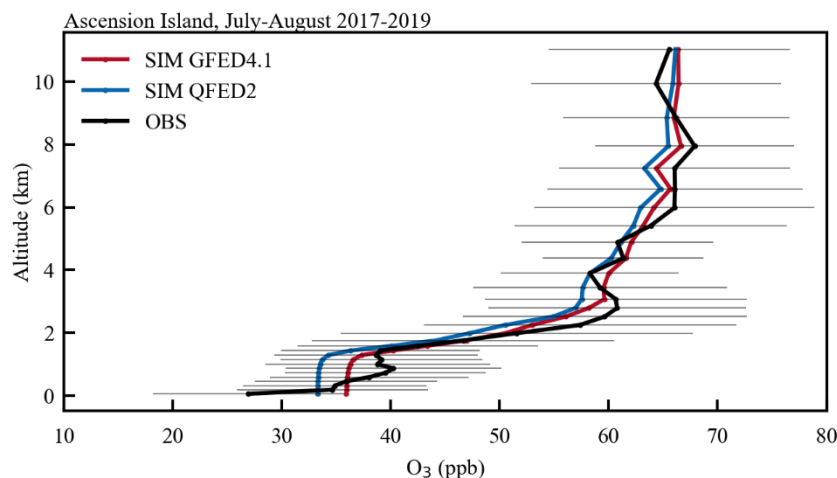
Figure 6. The comparison of GEOS-Chem simulated and measured vertical ozone distributions over the Ascension Island, UK, for July-August 2017-2019. The model results by the GFED4.1 (red) and QFED2 (blue) inventories are both given.

HCHO is one of the important VOCs in the troposphere, and a comparison of simulated and satellite-derived tropospheric HCHO columns is given in **Figures 5g-5i**. The HCHO column concentrations simulated by GEOS-Chem and the satellite observations exceeded 20×10^{15} molecule cm^{-2} in northern Angola and southwest DRC, and the underestimated HCHO columns in GEOS-Chem might be due to some missing VOC species (Zhao et al., 2024) and the lower anthropogenic NO$_x$ emissions in Southern Africa that both affect the chemical production of HCHO. Simulated HCHO column concentrations between the GFED4.1 and QFED2 inventories were consistent spatially, with only a difference of 1×10^{15} molecule cm^{-2} on a regional basis. The levels and spatial distributions of HCHO are mainly influenced by BVOC and BB emissions. Firstly, the Congo Basin, as one of the largest tropical rainforests, emits a large amount of BVOCs that can be oxidized to generate high values of HCHO (Wells et al., 2020). It leads to the spatial distribution of HCHO similar to the distribution of BVOC sources. Secondly, BB is found to be one of the main sources of HCHO in the African continent (Liu et al., 2020). Differences in VOC and NO$_x$ emissions between GFED4 and QFED inventories (Van Der Werf et al., 2017), e.g., BB VOC emissions in GFED4.1 being two times of the QFED2 inventory in 2019, may account for the slightly different HCHO columns.

The simulated CO columns in **Figures 5j-5l** are spatially similar to MOPPIT retrievals, with high values in the downwind regions of fire sources. The regional average of CO column concentrations simulated by GEOS-Chem is underestimated by approximately 10% compared to MOPITT, which reflects a long-lasting issue of CO underestimation in GEOS-Chem model (David et al., 2019; Ni et al., 2018). Hoelzemann (2006) used a variety of BB emission inventories to drive the

17

MOZART model to simulate CO concentrations in Southern Africa in September-October 2000, and they showed that all simulations exhibited an underestimation against the MOPITT CO. In addition, we also found that the simulated spatial distribution of CO columns is similar with each other among different BB inventories, and their regional difference is only 1%. This suggests that neither HCHO nor CO is the main reason for the overestimation of ozone production.
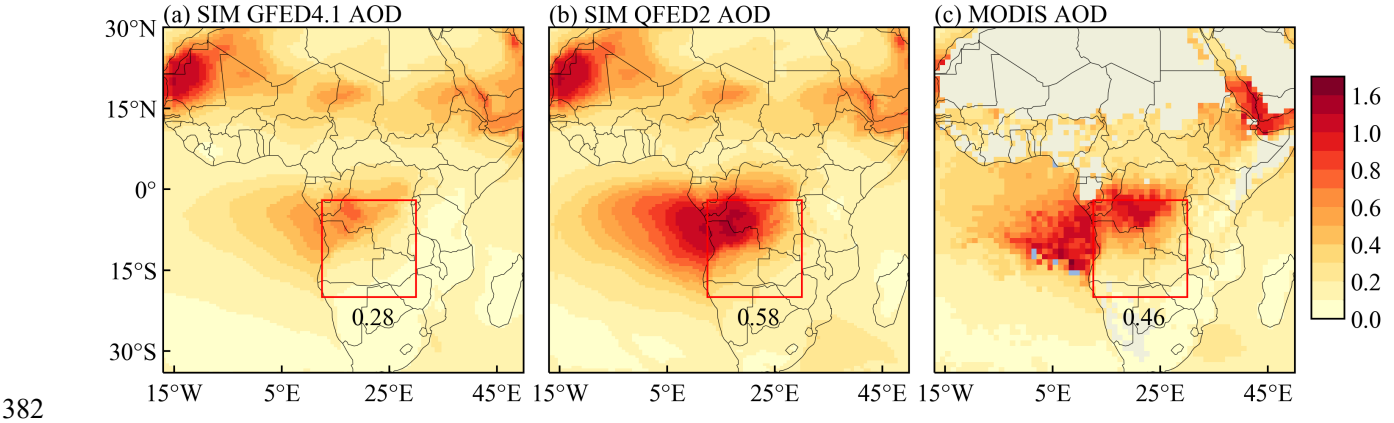
Figure 7. The comparison of GEOS-Chem simulated AOD in Africa in July-August 2019 with the MODIS AOD. The model results by the GFED4.1 (left) and QFED2 (middle) inventories are both given.

We compared the spatial distribution of modeled and satellite-based AOD as shown in **Figure 7**. The simulation results by both inventories can capture the spatial variability of MODSI AOD. But simulated regional mean AOD by the QFED2 inventory overestimated MODIS AOD by 26%, while the GFED4.1 inventory underestimated MODIS AOD by 37%. Tian et al. (2019) used GFED4 as an input to drive the GEOS-Chem model and also showed that the model tended to underestimate the intensity and spatial distribution of AOD in the African region. The inconsistency between these two inventories may be attributed to the discrepancy in carbonaceous aerosol emissions, since the OC and BC emissions from GFED4 are only half of the QFED emissions (Chang et al., 2023). In addition, the difference between OC and BC in the biomass burning emission inventories could affect ozone simulation through aerosol chemistry, and the results are shown in **Figure S10**. Aerosol chemistry mainly influences ozone formation by altering photolysis and heterogeneous processes. On the one hand, aerosol can change the shortwave radiation reaching the ground through scattering and absorption, which in turn affects the photolysis rate. On the other hand, aerosol can update reactive radicals (e.g., HO_2, nitrogen radicals) that are critical for ozone formation. After turning off aerosol chemistry alone in the model, regional surface ozone was increased by 10 ppb and TCO by 2 DU using the GFED4.1, while using the QFED2 regional ozone was increased by 14 ppb and TCO by 4 DU. As such, the lower level of aerosols in GFED4.1 may be a reason for the overestimation of simulated ozone concentrations.

18

402   In conclusion, the widely-used GFED4.1 inventory has a large bias in simulating tropospheric ozone in Southern Africa,

403   and the QFED2 inventory exhibit much more consistent with satellite observations in terms of simulated concentration

404   levels and spatial distributions (Table S1). This bias is mainly due to the overestimation of NO_x emissions in Southern

405   Africa in GFED4.1. Firstly, NO_x emissions in GFED4.1 are 38% higher than in QFED2 in Southern Africa. Secondly, the

406   modeled NO_2 column in GFED4.1 shows a high bias compared to QFED2 and satellite observations, while the modeled

407   HCHO and CO columns are generally consistent between GFED4.1 and QFED2 inventories. Thus, we conclude that the

408   overestimation of ozone in Southern Africa simulated with GFED4.1 is due mainly to the overestimation of NO_x and the

409   lower aerosol levels in GFED4.1 may be a minor reason for the overestimation of modeled ozone concentrations. We will

410   use the QFED2 inventory for BB emissions in the following analysis.

411   **3.2.4 Role of BB emission heights in ozone simulation**

412   The representativeness of BB emission injection heights is also an important factor that can impact ozone simulations

413   (Rémy et al., 2017). We conducted a sensitivity experiment using the QFED2 inventory and allowed all BB emissions

414   emitting below the PBL. As shown in **Figure 8**, the impact of this vertical partitioning on surface ozone varies regionally.

415   At the surface, the changes of MDA8 ozone were within ± 2.4 ppb and the BB source areas showed a decreased ozone. For

416   TCO, the simulated mean values with this vertical partitioning were 0.2 DU higher than those without vertical partitioning,

417   but the magnitude of this effect is smaller than the TCO changes (~4 DU) caused by the difference in BB NO_x emissions

418   between GFED4.1 and QFED2 inventories. Thus, our simulations demonstrate that the configuration of BB emission height

419   has a limited effect on surface ozone level but a moderate influence on TCO columns in this region.

420   **3.3 Impacts of anthropogenic emissions on tropospheric ozone**

421   **3.3.1 Uncertainties in anthropogenic emission inventories**

422   Uncertainties may exist in anthropogenic emissions from regional scale to urban cities in Southern Africa. For example, in

423   **Table 3** we compared the differences in NO_x emissions between two widely-used global inventories: Community

424   Emissions Data System (CEDSv2) and HTAPv3. Whether in Southern Africa or Luanda, there is a missing seasonality

425   in NO_x emissions in CEDSv2, whereas NO_x emissions in HTAPv3 are much higher in January-February than in other

426   months. Over the Southern Africa, monthly NO_x emissions in the CEDSv2 are about 30% lower than the HTAPv3 in

427   January-February. For Luanda, the CEDSv2 inventory is 87% lower than HTAPv3 in January-February 2018 and 20-50%

428   lower in the other months. In addition, the validation of anthropogenic emission in global inventories was barely evaluated

429   in this region and we will take advantage of recently available surface measurements and satellite retrievals to fill this gap.

430 **3.3.2 Model evaluation against surface measurements of NO₂ and PM₂.₅**

431 Currently, there are very few surface observations in Southern Africa. However, in the study, there are three cities
432 (Humpata, Luanda, and Luena) that have continuous surface measurements of NO₂ during the period of June-August 2023,
433 and four cities (Humpata, Luanda, Luena, and Lusaka) with surface measurements of PM₂.₅. These measurements are
434 critical to understand the hotspots of urban anthropogenic emissions as indicated in **Figure 2a**. Luanda is the capital of
435 Angola with dense population, and the median surface NO₂ concentrations observed at this station ranged from 10 ppb to
436 30 ppb. The
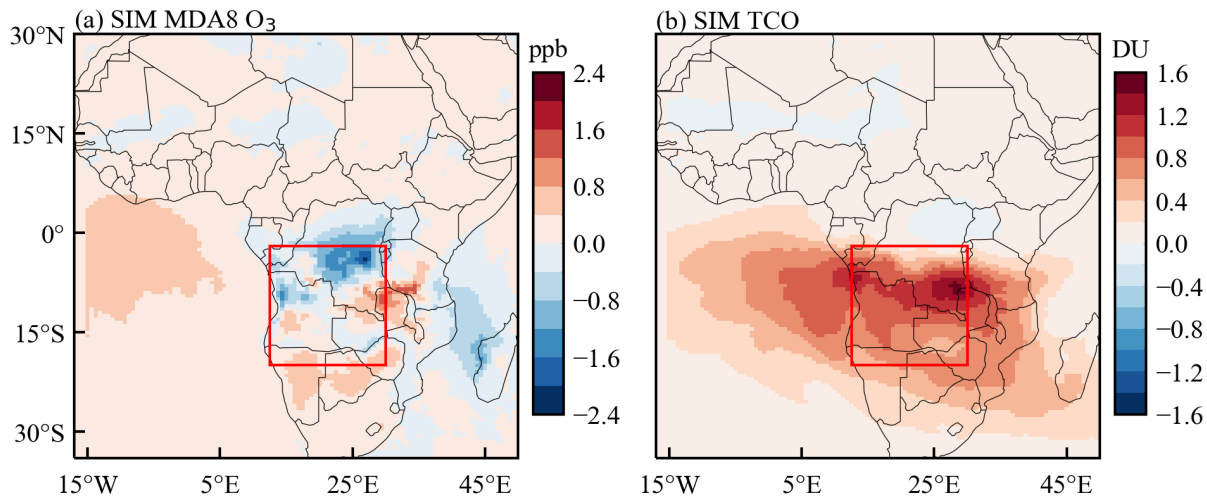
437
438 **Figure 8.** Effects of vertical partitioning of model BB emissions in surface MDA8 ozone and tropospheric ozone columns.
439 The baseline simulation follows the vertical distribution of QFED2 emission (i.e., 65% emissions below the PBL and 35%
440 emissions into the free atmosphere), and the sensitivity simulation allows 100% BB emissions emitted below the PBL.
441 Here the plots are the differences between the baseline simulation (Run_QFED) and sensitivity simulation
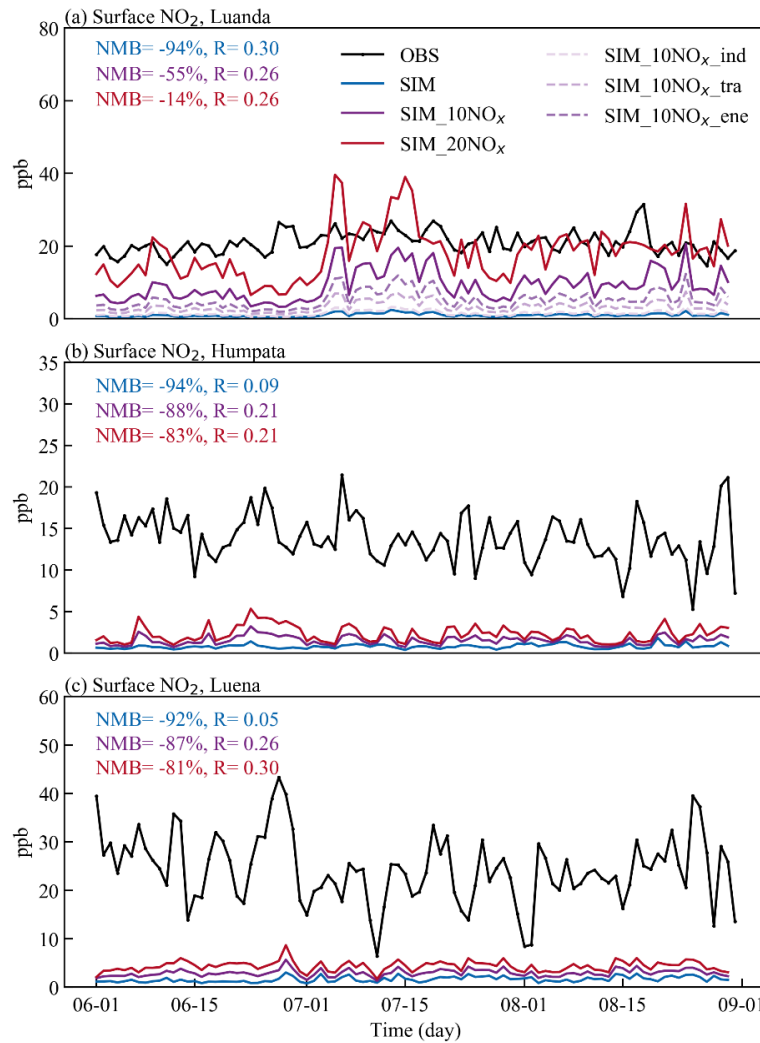442 (Run_QFED_PBL).

443

444

445

446

447
448

449 **Table 3.** Monthly anthropogenic NO$_x$ emissions in Southern Africa and Luanda (unit: Gg month^{-1}).

		Jan.	Feb.	Mar.	Apr.	May	Jun.	Jul.	Aug.	Sep.	Oct.	Nov.	Dec.
Southern Africa	CEDSv2	18.2	16.5	18.2	17.6	18.2	17.6	18.2	18.2	17.6	18.2	17.6	18.2
	HTAPv3	27.1	24.9	17.6	17.0	17.3	18.9	19.0	17.1	16.7	17.8	17.0	16.4
Luanda	CEDSv2	0.8	0.7	0.8	0.8	0.8	0.8	0.8	0.8	0.8	0.8	0.8	0.8
	HTAPv3	6.3	5.2	1.5	1.0	1.2	1.1	1.1	1.2	1.0	1.3	1.2	1.0

450

451 Humpata station is located at Universidade Privada de Angola, where the observed NO$_2$ concentrations ranged from 5 ppb
452 to 25 ppb, with large day-to-day variations of up to 20 ppb. The Luena station is located in a residential area of Luena,
453 where the observed NO$_2$ concentrations were much higher than those of the previous two stations, with a maximum of 50
454 ppb. **Figure 9** shows the comparison of the observed and simulated daily surface NO$_2$ concentrations in Luanda, Humpata,
455 and Luena, respectively. Compared with the observed values, the modeled NO$_2$ concentrations for all three cities are much
456 lower than the observed values, underestimated by 90%. There is also a large underestimation of surface NO$_2$ in Luanda
457 compared to the observations from Campos et al. (2021). This indicates that urban NO$_x$ emissions in our model are highly
458 underestimated in Southern Africa, although the lack of model resolution accuracy is also a reason for the underestimation
459 at the station scale.

460

461 To test the sensitivity of simulated NO$_2$ concentration to urban emissions, we increased the NO$_x$ emissions in the CEDSv2
462 inventory by a factor of 10, and the model results are shown in **Figure 9**. In Luanda, the Normalized Mean Bias (NMB) of
463 simulated NO$_2$ concentrations will be decreased from -94% in the baseline simulation to -55%, while the changes of NO$_2$
464 in Humpata and Luena are very limited with an improvement of the NMB of only 5%. Even if when NO$_x$ emission is scaled
465 up by a factor of 20, the simulated NO$_2$ concentrations in Humpata and Luena are increased by only 11-21%. For Luanda,
466 there is a NMB of -50% in modeled surface NO$_2$ with 10-fold NO$_x$ emissions. But for Humpata and Luena, the CEDSv2
467 inventory is not capable to correctly estimate the anthropogenic sources, leading to the small sensitivity of simulated NO$_2$
468 concentration to perturbed urban emissions.

469
470
471
472
473
474

(a) Surface NO$_2$, Luanda

NMB= -94%, R= 0.30
NMB= -55%, R= 0.26
NMB= -14%, R= 0.26

(b) Surface NO$_2$, Humpata

NMB= -94%, R= 0.09
NMB= -88%, R= 0.21
NMB= -83%, R= 0.21

(c) Surface NO$_2$, Luena

NMB= -92%, R= 0.05
NMB= -87%, R= 0.26
NMB= -81%, R= 0.30

Legend: OBS, SIM, SIM_10NO$_x$, SIM_20NO$_x$, SIM_10NO$_x$_ind, SIM_10NO$_x$_tra, SIM_10NO$_x$_ene

475

Figure 9. Time series of simulated and observed daily median surface NO$_2$ concentrations in Southern African cities (Luanda, Humpata, Luena) in June-August 2023. The model was driven by the QFED2 inventory and fixed CEDSv2 inventory in 2019. The "SIM" denotes the baseline simulation (Run_QFED_2023), and "SIM_10NO$_x$", and "SIM_20NO$_x$" denote the 10-fold and 20-fold increase in NO$_x$ emissions from CEDSv2. The dashed lines indicate a 10-fold increase in NO$_x$ emissions from the energy (ene), industry (ind) and transportation (tra) sectors, respectively, in the CEDSv2 inventory.

Although this study focused on ozone simulation, the comparison of model results against the valuable PM$_{2.5}$ measurements will be also meaningful to understand urban emissions in this region. **Figure 10** shows the time series of observed and simulated PM$_{2.5}$ concentrations in June-August 2023. The PM$_{2.5}$ concentrations observed at both the Humpata and Luanda

22
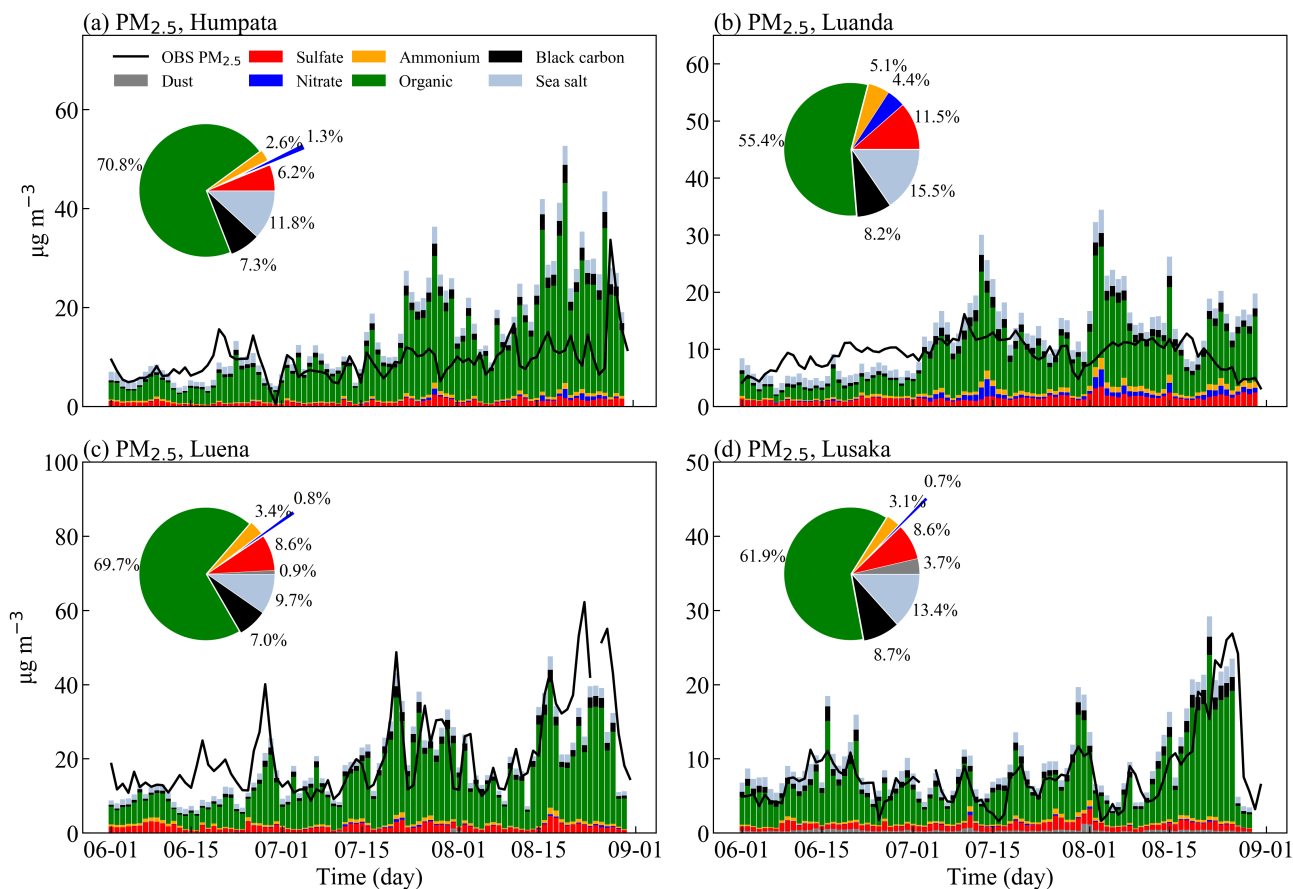
Figure 10. Comparison of simulated time series of $PM_{2.5}$ and its components against with the observed $PM_{2.5}$ (black line) during June-August 2023. (a) and (b) are for Humpata and Luanda, respectively, where we removed dust concentrations from the simulated $PM_{2.5}$ due to the large uncertainties in the model, and (c) and (d) are for Luena and Lusaka, respectively. The pie charts show the percentage contributions of each component to total $PM_{2.5}$ concentrations.

sites were around 10 μg m^{-3}. The $PM_{2.5}$ concentrations at the Luena site were slightly higher compared to the other two sites, with median concentrations ranging from 10 μg m^{-3} to 70 μg m^{-3}. Lusaka is the capital of Zambia and the observed site is located within the urban area of Lusaka, where $PM_{2.5}$ concentrations were about 10 μg m^{-3} in June-July and then suddenly increased to about 20 μg m^{-3} in August. **Figure S11** shows the comparison of simulated and observed $PM_{2.5}$ concentrations, and the model can capture the day-to-day variation in $PM_{2.5}$ concentrations at Luena as well as Lusaka sites, with NMBs of -12% and 24% and correlation coefficients of 0.7 and 0.87, respectively. But in Luanda and Humpata, there is a large overestimation in simulated $PM_{2.5}$ concentration and a large proportion of $PM_{2.5}$ components is contributed by dust, possibly due to the influence of the Namib and Kalahari Deserts (Nyasulu et al., 2023). We excluded dust

499 concentration in the calculation of total $PM_{2.5}$ concentration for the time being, due to its large uncertainties in the GEOS-

500 Chem simulation (Weagle et al., 2018). After removing dust concentration, the NMB in the model will be reduced from

501 149% to 37% in Luanda.

502

503 In terms of $PM_{2.5}$ components, the highest contribution of OC to $PM_{2.5}$ concentrations is found at all the four sites, which

504 can be attributed to the effects from biomass burning (Nyasulu et al., 2023). Secondary inorganic aerosols account for

505 about 20% at Luanda and about 10% at other sites. In addition, we also compared the changes in $PM_{2.5}$ concentrations at

506 each site after scaling up anthropogenic NO_x emissions by a factor of 10, and found that $PM_{2.5}$ at the Luanda site can

507 increase by up to 50 μg m^{-3}. In previous studies, changes in $PM_{2.5}$ concentrations in Southern Africa have often been

508 attributed to BB (Nyasulu et al., 2023; Booyens et al., 2019). However, this study shows that anthropogenic emissions in

509 Luanda could also have a great impact on $PM_{2.5}$ concentrations, highlighting the underappreciated role of anthropogenic

510 emissions in urban air quality over the Southern Africa.

511

512 We further explored the sensitivity of ozone concentration to perturbed NO_x emissions. **Figure S12** shows the response of

513 ozone concentration at each site after anthropogenic NO_x was increased by 10 times. Relative to the baseline run, the ten-

514 fold NO_x simulation can increase ozone concentrations by 0-10 ppb in the Humpata and Luean regions. However, in Luanda

515 there was increased ozone in June but decreased ozone in July-August in response to ten-fold NO_x emissions, indicating

516 that ozone chemistry in Luanda may be likely shift into transition regime with increasing emissions. Again, these results

517 confirm that the underestimation of anthropogenic emissions in the urban areas of Southern Africa now can have an

518 important impact on local ozone assessment.

519

520 Although there is a lack of surface ozone observations in Southern Africa that can be directly compared with our model

521 results, we can conclude from the model evaluation against surface NO_2 and $PM_{2.5}$ measurements: 1) the large

522 underestimation in modeled urban scale NO_2 in Southern Africa is mainly due to large low biases of NO_x emission in the

523 CEDSv2 inventory, i.e., a strong underestimation in Luanda and the misrepresentation of anthropogenic emission estimates

524 in Humpata and Luena, 2) the model is able to capture the observed variations in $PM_{2.5}$ concentrations in the areas that are

525 less affected by dust, and 3) the bias in anthropogenic emission inventories can strongly affect the assessment of $PM_{2.5}$ and

526 ozone concentrations in urban Southern Africa.

527 **3.3.3 Model evaluation against satellite measurements**

528 Satellite observations were further used to support the deduction of the underestimated urban emissions. As the capital of

529 Angola, Luanda is of much higher anthropogenic emissions compared to other cities in Southern Africa. In the following,

we focused on Luanda where satellite signals could be stronger to detect NO_x emissions. **Figure 11** shows the simulated and satellite-based NO_2 columns for fire season (July-August 2019) and non-fire season (January-February 2020), respectively. To minimize the effects from background levels, here the NO_2 values are the columns at Luanda minus the mean columns averaged over the sea downwind. For July-August 2019, the urban NO_2 enhancement in Luanda simulated by the model was 26% lower than that observed by the TROPOMI; for January-February 2020, the simulated NO_2 enhancement was underestimated by 61% compared to TROPOMI. Due to the decreased contribution from anthropogenic sources to NO_2 columns during the fire season, the moderate underestimation during fire season (July-August 2019) in Luanda may be due to the long-term transport of pollutants from biomass burning to urban areas. As suggested by TROPOMI satellite, therefore, NO_x emissions from CEDSv2 were underestimated by at least a factor of 2 in urban Luanda. At the same time, we find that the NO_2 enhancement in Luanda observed by OMI was 70% lower compared to TROPOMI and the OMI instrument cannot detect the high emissions in Luanda, demonstrating the advantage of TROPOMI instrument in observing regions with significant NO_x spatial heterogeneity.
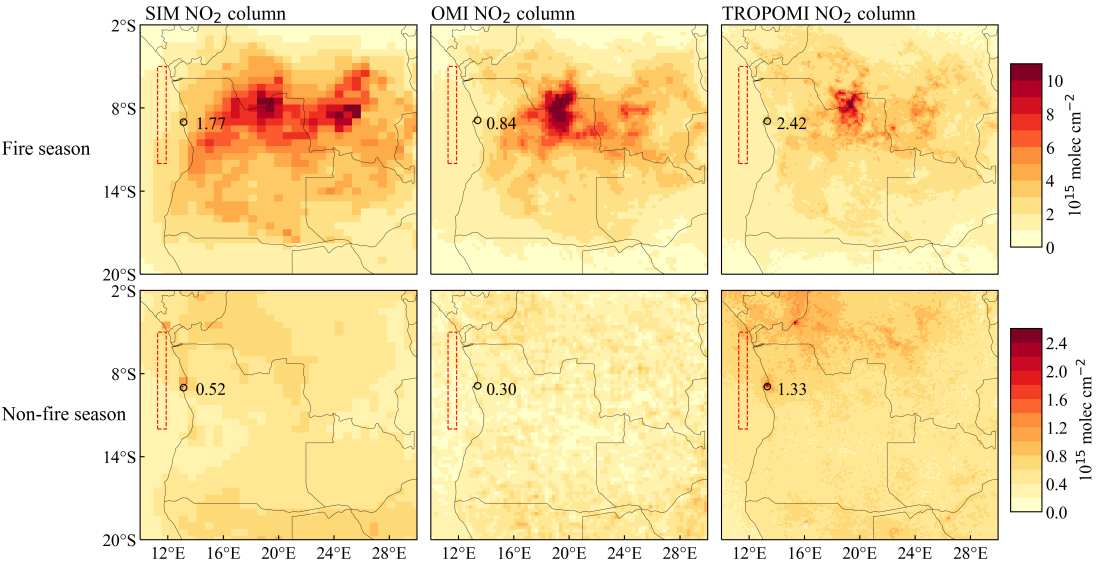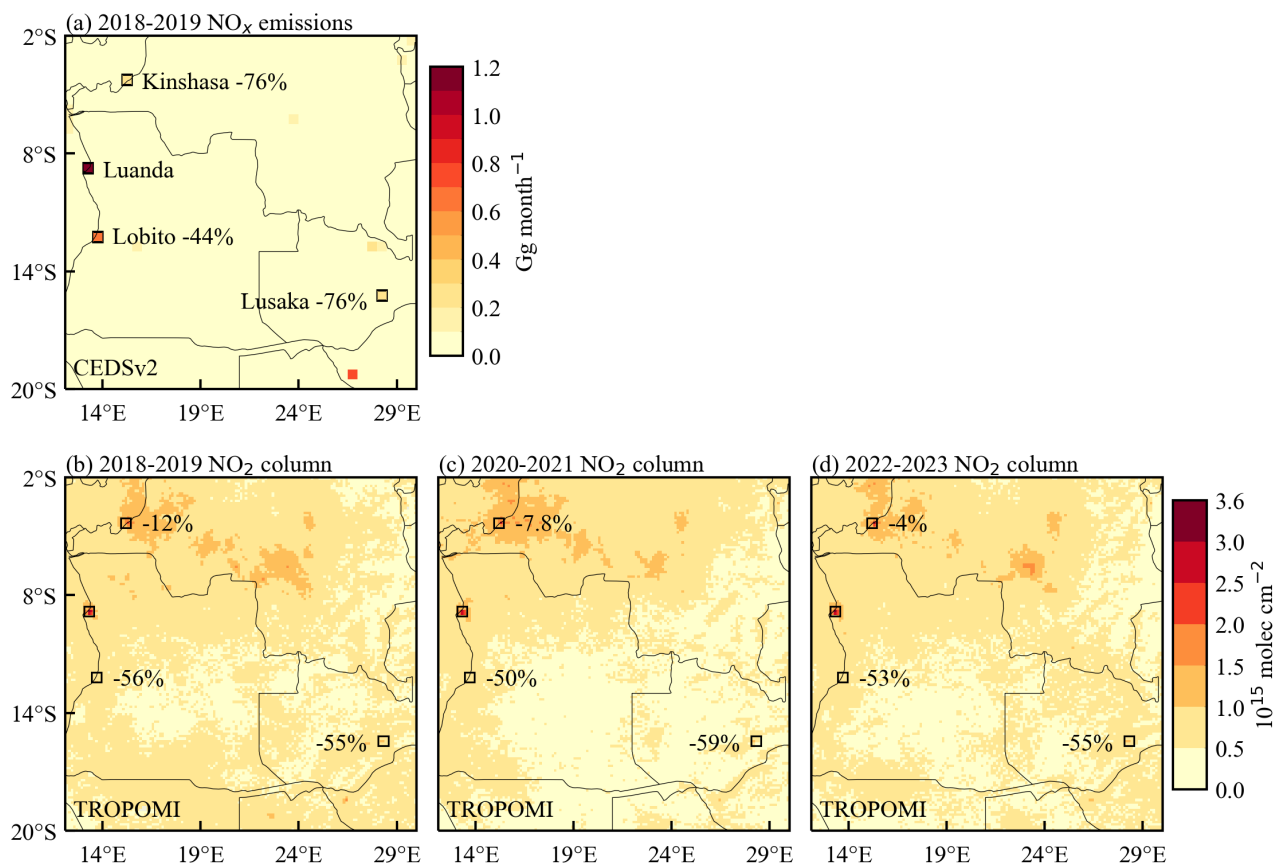

Figure 11. Spatial distribution of NO_2 columns from the model, OMI, and TROPOMI during the fire season (top, July-August 2019) and non-fire season (bottom, January-February 2020). Circles indicate the Luanda city and numbers around them indicate NO_2 column enhancement in the Luanda city. The dashed boxes indicate the downwind ocean region whose concentrations were subtracted to obtain the NO_2 column enhancement in Luanda.

To further identify the key emission sectors in Luanda, we perturbed the NO_x emissions from three sectors (transportation,

550 industrial, and energy) by a factor of 10 in **Figure 9a**. Surface NO_2 concentrations in Luanda responded better to changes
551 in NO_x emissions from the energy and transportation sectors, with NMB reduced by 20% and 11%, respectively. **Figure**
552 **S13** shows the NO_2 column changes in response to the emission perturbations. When all sources of NO_x emissions in the
553 CEDSv2 inventory were increased by a factor of 10, the simulated NO_2 column enhancement in Luanda will be 3-4 times
554 the TROPOMI measurement. Namely, the ten-fold increase in NO_x emissions to be consistent with surface measurement
555 cannot reconcile with satellite measurements. In addition, the response of NO_2 column in Luanda to sectoral perturbations
556 in NO_x emissions is mainly linear (**Figure S13**). These model-satellite comparisons suggest an underestimation of NO_x
557 emissions from CEDSv2 by at least a factor of 2 in urban Luanda.

558

559 To further explore the underestimation of anthropogenic emissions in Southern Africa, we use Luanda as a baseline to
560 show the difference between anthropogenic NO_x emissions and satellite NO_2 columns for other cities in **Figure 12**. The
561 selected cities are grid cells with high NO_x emissions in the CEDSv2 inventory. The tropospheric NO_2 during non-fire
562 season is dominantly contributed by the lower atmosphere (**Figure S14**), and then we selected March-April 2018-2023 for
563 comparison in order to exclude the effect of biomass burning. In Kinshasa (the capital of the DRC), anthropogenic NO_x
564 emissions are 76% lower than those in Luanda, but their difference in satellite NO_2 columns was only 4-12%, suggesting
565 that anthropogenic emissions from Kinshasa were also underestimated; In Lusaka (the capital of Zambia), its NO_2 columns
566 were 55 % lower than those in Luanda while the difference is 76% in anthropogenic NO_x emissions. Combining satellite
567 data with CEDSv2 NO_2 emissions provides additional evidence of the prevalent underestimation in anthropogenic NO_x
568 emissions in major cities over Southern Africa.

Figure 12. Anthropogenic NO_x emissions from CEDSv2 and NO_2 columns from TROPOMI in typical cities in Southern Africa. (a) Spatial distribution of NO_x emissions from the CEDSv2 inventory in March-April of 2018-2019. (b-d) Spatial distribution of NO_2 columns observed by TROPOMI in March-April, 2018-2023. All of the numbers in the plots are the percentage changes by taking Luanda as a reference.

4. Conclusions and discussion

In this study, we focused on Southern Africa where tropospheric ozone levels were thought extremely high but have been less studied. By integrating the nested GEOS-Chem model and the newly-available surface and satellite observations to evaluate the tropospheric ozone and its main drivers in Southern Africa. In particular, we quantified the impact of biomass burning (BB) on tropospheric ozone at the regional scale in Southern Africa and the effects of anthropogenic emissions in urban ozone level. This study provides a better understanding of the impacts of key emission sources on air quality modeling in Southern Africa, which will be also important for health risk assessment, climate change prediction, and

27

581   sustainable strategy development.

582

583   The anomalously high values of dry-season tropospheric ozone in Southern Africa are mainly caused by BB, but there is a

584   large discrepancy of a factor of 2-3 in estimated BB emissions among different inventories. Comparison of model

585   simulations against NO_2 satellite observations revealed that the widely-used GFED4.1 inventory tends to strongly

586   overestimate NO_x emissions in Southern Africa, while model results with the QFED2 inventory were more consistent with

587   observations. This is consistent with the finding by Anderson et al. (2021) that their model driven by the GFED4.1 inventory

588   tended to overestimate NO_2 concentrations in the Africa , with a bias of about 100%. Consequently, the simulated regional

589   surface MDA8 ozone was decreased from 74 ppb by GFED4.1 inventory to 56 ppb by QFED2 inventory, and accordingly

590   the model bias in TCO was reduced from 14% to 2.3%. The modeled HCHO and CO columns are consistent between

591   GFED4.1 and QFED2 inventories. Using the QFED2 inventory, we explored the impact of BB emission heights on ozone

592   simulations and found that the effect of the vertical emission distribution was in the range of ± 2.4 ppb for surface MDA8

593   ozone and from -0.4 to 1.6 DU for TCO over Southern Africa; in contrast, the difference in BB aerosol emissions between

594   the inventories could affect ozone simulation strongly through aerosol chemistry.

595

596   We conducted further sensitivity experiments using the QFED2 inventory to explore the contribution of anthropogenic

597   emissions. Compared with surface NO_2 and $PM_{2.5}$ observations, we found that the CEDSv2 anthropogenic inventory likely

598   strongly underestimated anthropogenic emissions in typical Southern African cities and even incorrectly represented

599   anthropogenic sources in some areas. Our study also found that the TROPOMI performs effectively in these low emission

600   areas where there is a lack of observational data, and the OMI instrument is unable to capture urban-scale hotspots in NO_2

601   columns over Southern Africa. We also demonstrated that urban ozone and $PM_{2.5}$ concentrations are strongly influenced

602   by the underestimated anthropogenic emissions. For example, a ten-fold increase in anthropogenic NO_x emissions can

603   change ozone concentrations by up to 10 ppb and increase $PM_{2.5}$ concentrations by up to 50 μg m^{-3} in some cities.

604

605   Although several studies examined high ozone levels in Southern Africa (Meyer-Arnek et al., 2005; V. Clarmann et al.,

606   2007), they only highlighted the role of biomass burning but overlooked the role of anthropogenic emissions. Although

607   recent findings by Wiedinmyer et al. (2023) have pointed out the large uncertainties in bottom-up BB emissions, they failed

608   to constrain the uncertainties due to the lack of observational data. Here we found that the difference among BB inventories

609   can have a great impact on urban air quality assessment. In addition, with combined surface observations, satellite data and

610   model simulations, we demonstrated for the first time that anthropogenic emission inventories are strongly low-biased in

611   urban Southern Africa. It suggests the important impacts of anthropogenic emissions in Africa with increasing urbanization.

612

613 The rapid change in anthropogenic emissions is already affecting air pollution and health risks in Southern Africa (Health
614 Effects Institute, 2022), as well as might have impacts on regional climate change (Fotso-Nguemo et al., 2023). Assessing
615 and predicting the impacts of different emission sources on air quality and human health rely heavily on model simulations.
616 The performance of these model estimations is significantly influenced by the accuracy of emission inventories. For
617 example, our finding of overestimated biomass burning emissions and underestimated anthropogenic emissions can
618 strongly affect the ozone source attribution over Southern Africa due to the nonlinear ozone chemistry. As shown in **Figure**
619 **S15**, in the dry season of 2019, regional surface MDA8 ozone over Southern Africa was contributed by 11 ppb, 8.0 ppb,
620 and 1.5 ppb from BB emissions, natural emissions (mainly biogenic VOC), and anthropogenic emissions, respectively.
621 However, when anthropogenic NO_x emissions were increased by a factor of 10, estimated contributions from natural and
622 anthropogenic emissions will be increased to 9.0 ppb and 3.3 ppb, respectively. In particular, the ozone source attribution
623 spatially varies depending on the levels of anthropogenic NO_x emissions (**Figure 13**). This suggests the ignored but critical
624 role of anthropogenic emissions in ozone levels over Southern Africa.
625
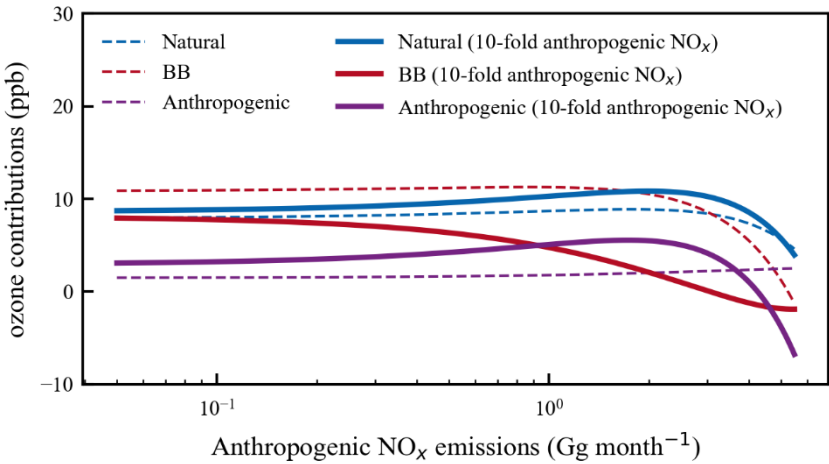
627 **Figure 13.** The simulated source contributions to surface ozone in July-August 2019 using the CEDSv2 emissions (dash
628 lines) and 10-fold CEDSv2 NO_x emissions (solid lines). Here the natural emissions refer to the biogenic VOC and soil NO_x
629 emissions. The x-axis is the anthropogenic NO_x emissions in each grid cell and the y-axis the corresponding ozone
630 contributions estimated from the sensitivity simulations.
631

632 There are also some uncertainties and limitations in our assessment of the major drivers of high ozone over Southern Africa.
633 Firstly, due to the lack of observational data on surface ozone and VOCs, the effect of anthropogenic emissions on surface
634 ozone over Southern Africa was explored by only comparing surface NO_2 concentrations, which may lead to biases in
635 determining ozone chemical formation. Secondly, although we have used ozonesonde data from Ascension Island

636 downwind of Southern Africa for comparison and the study by Jenkins et al. (2021) suggests that BB plumes in Southern
637 Africa can have an impact on downwind regions, the long-range effects of BB emission on downwind urban regions were
638 also not well validated due to the lack of vertical ozone measurement. Thirdly, the comparison between the model and
639 satellite data could be improved by correcting the vertical profiles of chemical species in the process of satellite data.
640 Fourthly, although the GEOS-Chem model has been shown to be able to capture spatial and temporal variations of ozone
641 and its precursors over typical urban regions (Travis and Jacob, 2019), it is still challenging to capture the urban scale air
642 quality in Southern Africa. Without accurate bottom-up anthropogenic inventories, we highlight the importance of high-
643 resolution satellite observations for understanding air quality in developing regions such as Southern Africa.

644

645 Overall, this work provides a comprehensive understanding of the drivers and uncertainties of tropospheric ozone in
646 Southern Africa, particularly the overestimation in BB emissions and the underestimation of anthropogenic emission
647 inventories. More importantly, with more frequent BB and rising anthropogenic emissions in Africa, this study highlights
648 the urgency of establishing the surface network for air quality measurement over Southern Africa. The more accurate
649 estimates of anthropogenic emission sources and more regular surface observations are the key to understand atmospheric
650 chemistry over Southern Africa that is driven by rapidly changing anthropogenic and biomass burning emissions. The
651 deepened understanding of major emission sources in Southern Africa will not only help us to provide a solid scientific
652 basis for policymakers to effectively address air quality issues, but also will enhance the model capability to predict future
653 air quality and climate change. In the future, anthropogenic air pollutants (e.g., NO_x emissions) in Southern Africa under
654 future scenarios are projected to increase all the way by 2060 (**Figure S16**); along with more fires under a warming future,
655 Southern Africa will be a hotspot suffering from complex atmospheric chemistry and climate issues, presenting a grand
656 challenge to realize the Sustainable Development Goals for having a healthy, climate-friendly, and resilient development
657 in Africa. Our study serves as a baseline understanding of these key emission sources which are key drivers for modelling
658 future air quality, climate change, and their socioeconomic impacts.

659

660

661 **Data availability**. Daily real-time air quality indexes for NO_2 and $PM_{2.5}$ were obtained from the Worldwide Air Q
662 uality Index (https://aqicn.org/station). The Ascension Island's ozonesonde data from the Southern Hemisphere Addi
663 tional Ozone Sounding network (https://tropo.gsfc.nasa.gov/shadoz/). The OMI satellite data for O_3, NO_2 and HCH
664 O are available at https://disc.gsfc.nasa.gov/datasets/. The TROPOMI data for NO_2 are available at https://www.eart
665 hdata.nasa.gov/sensors/tropomi. The MODIS data for AOD are available at https://ladsweb.modaps.eosdis.nasa.gov/s
666 earch/. The MOPITT data for CO are available at https://giovanni.gsfc.nasa.gov/giovanni/.

667

References

Aghedo, A. M., Schultz, M. G., and Rast, S.: The influence of African air pollution on regional and global tropospheric ozone, Atmospheric Chemistry and Physics, 7, 1193-1212, https://doi.org/10.5194/acp-7-1193-2007, 2007.

Ahn, D. H., Choi, T., Kim, J., Park, S. S., Lee, Y. G., Kim, S.-J., and Koo, J.-H.: Southern Hemisphere mid- and high-latitudinal AOD, CO, NO2, and HCHO: spatiotemporal patterns revealed by satellite observations, Progress in Earth and Planetary Science, 6, 10.1186/s40645-019-0277-y, 2019.

Anderson, D. C., Duncan, B. N., Fiore, A. M., Baublitz, C. B., Follette-Cook, M. B., Nicely, J. M., and Wolfe, G. M.: Spatial and temporal variability in the hydroxyl (OH) radical: understanding the role of large-scale climate features and their influence on OH through its dynamical and photochemical drivers, Atmospheric Chemistry and Physics, 21, 6481-6508, https://doi.org/10.5194/acp-21-6481-2021, 2021.

Aucoin, C. and Bello-Schünemann, J.: African urban futures, Institute for Security Studies Papers, 2016, 1-36, https://hdl.handle.net/10520/EJC-b07eee7c0, 2016.

Balamurugan, V., Chen, J., Qu, Z., Bi, X., Gensheimer, J., Shekhar, A., Bhattacharjee, S., and Keutsch, F. N.: Tropospheric NO₂ and O₃ Response to COVID‐19 Lockdown Restrictions at the National and Urban Scales in Germany, Journal of Geophysical Research: Atmospheres, 126, https://doi.org/10.1029/2021JD035440, 2021.

Bian, H., Chin, M., Kawa, S. R., Duncan, B., Arellano, A., and Kasibhatla, P.: Sensitivity of global CO simulations to uncertainties in biomass burning sources, Journal of Geophysical Research: Atmospheres, 112, 10.1029/2006jd008376, 2007.

Booyens, W., Beukes, J. P., Van Zyl, P. G., Ruiz-Jimenez, J., Kopperi, M., Riekkola, M.-L., Josipovic, M., Vakkari, V., and Laakso, L.: Summary of research paper published in Journal of Atmospheric Chemistry titled: Assessment of polar organic aerosols at a regional background site in southern Africa, Clean Air Journal, 29, https://doi.org/10.17159/2410-972X/2019/v29n1a10, 2019.

Boschetti, L. and Roy, D. P.: Defining a fire year for reporting and analysis of global interannual fire variability, Journal of

703   Geophysical Research: Biogeosciences, 113, https://doi.org/10.1029/2008JG000686, 2008.

704 Bourgeois, I., Peischl, J., Neuman, J. A., Brown, S. S., Thompson, C. R., Aikin, K. C., Allen, H. M., Angot, H., Apel, E. C.,
705   Baublitz, C. B., Brewer, J. F., Campuzano-Jost, P., Commane, R., Crounse, J. D., Daube, B. C., DiGangi, J. P., Diskin,
706   G. S., Emmons, L. K., Fiore, A. M., Gkatzelis, G. I., Hills, A., Hornbrook, R. S., Huey, L. G., Jimenez, J. L., Kim, M.,
707   Lacey, F., McKain, K., Murray, L. T., Nault, B. A., Parrish, D. D., Ray, E., Sweeney, C., Tanner, D., Wofsy, S. C., and
708   Ryerson, T. B.: Large contribution of biomass burning emissions to ozone throughout the global remote troposphere,
709   Proceedings of the National Academy of Sciences, 118, https://doi.org/10.1073/pnas.2109628118, 2021.

710 Campos, P. M. D., Esteves, A. F., Leitão, A. A., and Pires, J. C. M.: Design of air quality monitoring network of Luanda,
711   Angola: Urban air pollution assessment, Atmospheric Pollution Research, 12, 101128,
712   https://doi.org/10.1016/j.apr.2021.101128, 2021.

713 Carter, T. S., Heald, C. L., Jimenez, J. L., Campuzano-Jost, P., Kondo, Y., Moteki, N., Schwarz, J. P., Wiedinmyer, C.,
714   Darmenov, A. S., da Silva, A. M., and Kaiser, J. W.: How emissions uncertainty influences the distribution and
715   radiative impacts of smoke from fires in North America, Atmospheric Chemistry and Physics, 20, 2073-2097,
716   10.5194/acp-20-2073-2020, 2020.

717 Chang, I., Gao, L., Flynn, C. J., Shinozuka, Y., Doherty, S. J., Diamond, M. S., Longo, K. M., Ferrada, G. A., Carmichael,
718   G. R., Castellanos, P., da Silva, A. M., Saide, P. E., Howes, C., Xue, Z., Mallet, M., Govindaraju, R., Wang, Q., Cheng,
719   Y., Feng, Y., Burton, S. P., Ferrare, R. A., LeBlanc, S. E., Kacenelenbogen, M. S., Pistone, K., Segal-Rozenhaimer,
720   M., Meyer, K. G., Ryoo, J.-M., Pfister, L., Adebiyi, A. A., Wood, R., Zuidema, P., Christopher, S. A., and Redemann,
721   J.: On the differences in the vertical distribution of modeled aerosol optical depth over the southeastern Atlantic,
722   Atmospheric Chemistry and Physics Discussions., 23, 4283-4309, https://doi.org/10.5194/acp-23-4283-2023, 2023.

723 Chen, Y., Hall, J., van Wees, D., Andela, N., Hantson, S., Giglio, L., van der Werf, G. R., Morton, D. C., and Randerson, J.
724   T.: Multi-decadal trends and variability in burned area from the fifth version of the Global Fire Emissions Database
725   (GFED5), Earth System Science Data, 15, 5227-5259, 10.5194/essd-15-5227-2023, 2023.

726 Dai, H., Liao, H., Li, K., Yue, X., Yang, Y., Zhu, J., Jin, J., Li, B., and Jiang, X.: Composited analyses of the chemical and
727   physical characteristics of co-polluted days by ozone and PM2.5 over 2013–2020 in the Beijing–Tianjin–Hebei region,
728   Atmospheric Chemistry and Physics, 23, 23-39, 10.5194/acp-23-23-2023, 2023.

729 David, L. M., Ravishankara, A. R., Brewer, J. F., Sauvage, B., Thouret, V., Venkataramani, S., and Sinha, V.: Tropospheric
730   ozone over the Indian subcontinent from 2000 to 2015: Data set and simulation using GEOS-Chem chemical transport
731   model, Atmospheric Environment, 219, 10.1016/j.atmosenv.2019.117039, 2019.

732 DeWitt, H. L., Gasore, J., Rupakheti, M., Potter, K. E., Prinn, R. G., Ndikubwimana, J. d. D., Nkusi, J., and Safari, B.:
733   Seasonal and diurnal variability in O_3, black carbon, and CO measured at the Rwanda Climate Observatory,
734   Atmospheric Chemistry and Physics, 19, 2063-2078, https://doi.org/10.5194/acp-19-2063-2019, 2019.

735 Fajersztajn, L., Veras, M., Barrozo, L. V., and Saldiva, P.: Air monitoring coverage in low-income countries: an
736   observational study, The Lancet, 384, https://doi.org/10.1016/s0140-6736(14)61877-8, 2014.

737 Fotso‐Nguemo, T. C., Weber, T., Diedhiou, A., Chouto, S., Vondou, D. A., Rechid, D., and Jacob, D.: Projected Impact
738   of Increased Global Warming on Heat Stress and Exposed Population Over Africa, Earth's Future, 11,
739   10.1029/2022ef003268, 2023.

740 Fu, Y., Li, R., Hu, J., Wang, Y., and Duan, J.: Investigating the impacts of satellite fire observation accuracy on the top-
741   down nitrogen oxides emission estimation in northeastern Asia, Environment International, 169, 107498,
742   https://doi.org/10.1016/j.envint.2022.107498, 2022.

743 Gaudel, A., Cooper, O. R., Chang, K.-L., Bourgeois, I., Ziemke, J. R., Strode, S. A., Oman, L. D., Sellitto, P., Nédélec, P.,
744   Blot, R., Thouret, V., and Granier, C.: Aircraft observations since the 1990s reveal increases of tropospheric ozone at

745   multiple locations across the Northern Hemisphere, Science Advances, 6, eaba8272,
746   https://doi.org/10.1126/sciadv.aba8272, 2020.

747 Guenther, A. B., Jiang, X., Heald, C. L., Sakulyanontvittaya, T., Duhl, T., Emmons, L. K., and Wang, X.: The Model of
748   Emissions of Gases and Aerosols from Nature version 2.1 (MEGAN2.1): an extended and updated framework for
749   modeling biogenic emissions, Geoscientific Model Development, 5, 1471-1492, https://doi.org/10.5194/gmd-5-1471-
750   2012, 2012.

751 Health Effects Institute: The state of air quality and health impacts in Africa. A report from the state of global air initiative,
752   2022.

753 Hickman, J. E., Andela, N., Tsigaridis, K., Galy-Lacaux, C., Ossohou, M., Dammers, E., Van Damme, M., Clarisse, L., and
754   Bauer, S. E.: Continental and Ecoregion‐Specific Drivers of Atmospheric NO_2 and NH_3 Seasonality Over Africa
755   Revealed by Satellite Observations, Global Biogeochemical Cycles, 35, e2020GB006916,
756   https://doi.org/10.1029/2020gb006916, 2021.

757 Hoelzemann, J. J.: Global Wildland Fire Emission Modeling for Atmospheric Chemistry Studies, 2006.

758 Hoesly, R. M., Smith, S. J., Feng, L., Klimont, Z., Janssens-Maenhout, G., Pitkanen, T., Seibert, J. J., Vu, L., Andres, R. J.,
759   Bolt, R. M., Bond, T. C., Dawidowski, L., Kholod, N., Kurokawa, J.-i., Li, M., Liu, L., Lu, Z., Moura, M. C. P.,
760   O'Rourke, P. R., and Zhang, Q.: Historical (1750–2014) anthropogenic emissions of reactive gases and aerosols from
761   the Community Emissions Data System (CEDS), Geoscientific Model Development, 11, 369-408,
762   https://doi.org/10.5194/gmd-11-369-2018, 2018.

763 Hua, W., Lou, S., Huang, X., Xue, L., Ding, K., Wang, Z., and Ding, A.: Diagnosing uncertainties in global biomass burning
764   emission inventories and their impact on modeled air pollutants, Atmospheric Chemistry and Physics, 24, 6787-6807,
765   10.5194/acp-24-6787-2024, 2024.

766 Jaffe, D. A. and Wigder, N. L.: Ozone production from wildfires: A critical review, Atmospheric Environment, 51, 1-10,
767   10.1016/j.atmosenv.2011.11.063, 2012.

768 Jenkins, G. S., de Castro, V., Cunha, B., Fontanez, I., and Holzworth, R.: The Evolution of the Wave‐One Ozone
769   Maximum During the 2017 LASIC Field Campaign at Ascension Island, Journal of Geophysical Research:
770   Atmospheres, 126, https://doi.org/10.1029/2020jd033972, 2021.

771 Jiang, Y., Zhou, L., and Raghavendra, A.: Observed changes in fire patterns and possible drivers over Central Africa,
772   Environmental Research Letters, 15, https://doi.org/10.1088/1748-9326/ab9db2, 2020.

773 Julien, B., Véronique, Y., Corinne, G.-L., Marcellin, A., Aristide, A., Sékou, K., Cathy, L., Eric, G., Christelle, C., Money,
774   O., Sylvain, G., and Julien, D.: A pilot study of gaseous pollutants' measurement (NO_2, SO_2, NH_3, HNO_3 and O_3) in
775   Abidjan, Côte d'Ivoire: contribution to an overview of gaseous pollution in African cities, Atmospheric Chemistry
776   and Physics, 18, 5173-5198, https://doi.org/10.5194/acp-18-5173-2018, 2018.

777 Kopacz, M., Jacob, D. J., Fisher, J. A., Logan, J. A., Zhang, L., Megretskaia, I. A., Yantosca, R. M., Singh, K., Henze, D.
778   K., Burrows, J. P., Buchwitz, M., Khlystova, I., McMillan, W. W., Gille, J. C., Edwards, D. P., Eldering, A., V. Thouret,
779   and Nedelec, P.: Global estimates of CO sources with high resolution by adjoint inversion of multiple satellite
780   datasets (MOPITT, AIRS, SCIAMACHY,TES), Atmospheric Chemistry and Physics, 10, 855–876, 2010.

781 Li, M., Yang, Y., Wang, H., Li, H., Wang, P., and Liao, H.: Summertime ozone pollution in China affected by stratospheric
782   quasi-biennial oscillation, Atmospheric Chemistry and Physics, 23, 1533-1544, https://doi.org/10.5194/acp-23-1533-
783   2023, 2023.

784 Liousse, C., Assamoi, E., Criqui, P., Granier, C., and Rosset, R.: Explosive growth in African combustion emissions from
785   2005 to 2030, Environmental Research Letters, 9, 035003, https://doi.org/10.1088/1748-9326/9/3/035003, 2014.

Liu, Y., Tang, Z., Abera, T., Zhang, X., Hakola, H., Pellikka, P., and Maeda, E.: Spatio-temporal distribution and source partitioning of formaldehyde over Ethiopia and Kenya, Atmospheric Environment, 237, https://doi.org/10.1016/j.atmosenv.2020.117706, 2020.

Liu, T., L.J. Mickley, M.E. Marlier, R.S. DeFries, M.F. Khan, M.T. Latif, and A. Karambelas.: Diagnosing spatial biases and uncertainties in global fire emissions inventories: Indonesia as regional case study. Remote Sensing of Environment, 237, 111557, https://doi.org/10.1016/j.rse.2019.111557, 2020

Lyu, X., Li, K., Guo, H., Morawska, L., Zhou, B., Zeren, Y., Jiang, F., Chen, C., Goldstein, A. H., Xu, X., Wang, T., Lu, X., Zhu, T., Querol, X., Chatani, S., Latif, M. T., Schuch, D., Sinha, V., Kumar, P., Mullins, B., Seguel, R., Shao, M., Xue, L., Wang, N., Chen, J., Gao, J., Chai, F., Simpson, I., Sinha, B., and Blake, D. R.: A synergistic ozone-climate control to address emerging ozone pollution challenges, One Earth, 6, 964-977, https://doi.org/10.1016/j.oneear.2023.07.004, 2023.

Marais, E. A. and Wiedinmyer, C.: Air Quality Impact of Diffuse and Inefficient Combustion Emissions in Africa (DICE-Africa), Environmental Science & Technology, 50, 10739-10745, https://doi.org/10.1021/acs.est.6b02602, 2016.

Mari, C. H., Cailley, G., Corre, L., Saunois, M., Attie, J. L., Thouret, V., and Stohl, A.: Tracing biomass burning plumes from the Southern Hemisphere during the AMMA 2006 wet season experiment, Atmospheric Chemistry and Physics, 8, 3951-3961, https://doi.org/10.5194/acp-8-3951-2008, 2008.

Marvin, M. R., Palmer, P. I., Latter, B. G., Siddans, R., Kerridge, B. J., Latif, M. T., and Khan, M. F.: Photochemical environment over Southeast Asia primed for hazardous ozone levels with influx of nitrogen oxides from seasonal biomass burning, Atmospheric Chemistry and Physics, 21, 1917-1935, https://doi.org/10.5194/acp-21-1917-2021, 2021.

Meyer-Arnek, J., Ladstätter-Weißenmayer, A., Richter, A., Wittrock, F., and Burrows, J. P.: A study of the trace gas columns of O_3, NO_2 and HCHO over Africa in September 1997, Faraday Discussions, 130, 387–405, https://doi.org/10.1039/b502106p, 2005.

Murray, C. J. L. and Aravkin, A. Y. and Zheng, P. and Abbafati, C. and Abbas, K. M. and Abbasi-Kangevari, M. and Abd-Allah, F. and Abdelalim, A. and Abdollahi, M. and Abdollahpour, I. and Abegaz, K. H. and Abolhassani, H. and Aboyans, V. and Abreu, L. G. and Abrigo, M. R. M. and Abualhasan, A. and Abu-Raddad, L. J. and Abushouk, A. I. and Adabi, M. and Adekanmbi, V. and Adeoye, A. M. and Adetokunboh, O. O. and Adham, D. and Advani, S. M. and Agarwal, G. and Aghamir, S. M. K. and Agrawal, A. and Ahmad, T. and Ahmadi, K. and Ahmadi, M. and Ahmadieh, H. and Ahmed, M. B. and Akalu, T. Y. and Akinyemi, R. O. and Akinyemiju, T. and Akombi, B. and Akunna, C. J. and Alahdab, F. and Al-Aly, Z. and Alam, K., et al.: Global burden of 87 risk factors in 204 countries and territories, 1990–2019: a systematic analysis for the Global Burden of Disease Study 2019, The Lancet, 396, 1223-1249, https://doi.org/10.1016/s0140-6736(20)30752-2, 2020.

Ni, R., Lin, J., Yan, Y., and Lin, W.: Foreign and domestic contributions to springtime ozone over China, Atmospheric Chemistry and Physics, 18, 11447-11469, 10.5194/acp-18-11447-2018, 2018.

Ni, Y., Yang, Y., Wang, H., Li, H., Li, M., Wang, P., Li, K., and Liao, H.: Contrasting changes in ozone during 2019–2021 between eastern and the other regions of China attributed to anthropogenic emissions and meteorological conditions, Science of The Total Environment, 908, 10.1016/j.scitotenv.2023.168272, 2024.

Nikonovas, T., North, P. R. J., and Doerr, S. H.: Particulate emissions from large North American wildfires estimated using a new top-down method, Atmospheric Chemistry and Physics, 17, 6423-6438, https://doi.org/10.5194/acp-17-6423-2017, 2017.

Nyasulu, M., Thulu, F. G. D., and Alexander, F.: An assessment of four decades atmospheric PM2.5 trends in urban locations over Southern Africa using MERRA-2 reanalysis, Air Quality, Atmosphere & Health, 16, 2063-2084, https://doi.org/10.1007/s11869-023-01392-3, 2023.

Park, R. J., Jacob, D. J., Field, B. D., and Yantosca, R. M.: Natural and transboundary pollution influences on sulfate-nitrate-ammonium aerosols in the United States: Implications for policy, Journal of Geophysical Research: Atmospheres, 109, 1-17, https://doi.org/10.1029/2003jd004473, 2004.

Pechony, O., Shindell, D. T., and Faluvegi, G.: Direct top-down estimates of biomass burning CO emissions using TES and MOPITT versus bottom-up GFED inventory, Journal of Geophysical Research: Atmospheres, 118, 8054-8066, https://doi.org/10.1002/jgrd.50624, 2013.

Petrenko, M., Kahn, R., Chin, M., Soja, A., Kucsera, T., and Harshvardhan: The use of satellite-measured aerosol optical depth to constrain biomass burning emissions source strength in the global model GOCART, Journal of Geophysical Research: Atmospheres, 117, 1-26, https://doi.org/10.1029/2012jd017870, 2012.

Qin, Y., Wang, H., Wang, Y., Lu, X., Tang, H., Zhang, J., Li, L., and Fan, S.: Wildfires in Southeast Asia pollute the atmosphere in the northern South China Sea, Science Bulletin, 69, 1011-1015, 10.1016/j.scib.2024.02.026, 2024.

Qu, Y., Wang, T., Wu, H., Shu, L., Li, M., Chen, P., Zhao, M., Li, S., Xie, M., Zhuang, B., Liu, J., and Han, Y.: Vertical structure and interaction of ozone and fine particulate matter in spring at Nanjing, China: The role of aerosol's radiation feedback, Atmospheric Environment, 222, 10.1016/j.atmosenv.2019.117162, 2020.

Rémy, S., Veira, A., Paugam, R., Sofiev, M., Kaiser, J. W., Marenco, F., Burton, S. P., Benedetti, A., Engelen, R. J., Ferrare, R., and Hair, J. W.: Two global data sets of daily fire emission injection heights since 2003, Atmospheric Chemistry and Physics, 17, 2921-2942, https://doi.org/10.5194/acp-17-2921-2017, 2017.

Roy, R.: The cost of air pollution in Africa, https://doi.org/10.1787/18151949, 2016.

Shi, H., Xiao, Z., Zhan, X., Ma, H., and Tian, X.: Evaluation of MODIS and two reanalysis aerosol optical depth products over AERONET sites, Atmospheric Research, 220, 75-80, 10.1016/j.atmosres.2019.01.009, 2019.

Shi, Y., Zang, S., Matsunaga, T., and Yamaguchi, Y.: A multi-year and high-resolution inventory of biomass burning emissions in tropical continents from 2001–2017 based on satellite observations, Journal of Cleaner Production, 270, https://doi.org/10.1016/j.jclepro.2020.122511, 2020.

Shi, Y., Matsunaga, T., Saito, M., Yamaguchi, Y., and Chen, X.: Comparison of global inventories of CO_2 emissions from biomass burning during 2002–2011 derived from multiple satellite products, Environmental Pollution, 206, 479-487, https://doi.org/10.1016/j.envpol.2015.08.009, 2015.

Sicard, P., Agathokleous, E., Anenberg, S. C., De Marco, A., Paoletti, E., and Calatayud, V.: Trends in urban air pollution over the last two decades: A global perspective, Science of The Total Environment, 858, 160064, https://doi.org/10.1016/j.scitotenv.2022.160064, 2023.

Souri, A. H., Duncan, B. N., Strode, S. A., Anderson, D. C., Manyin, M. E., Liu, J., Oman, L. D., Zhang, Z., and Weir, B.: Enhancing Long-Term Trend Simulation of Global Tropospheric OH and Its Drivers from 2005-2019: A Synergistic Integration of Model Simulations and Satellite Observations, EGUsphere, 1-37, https://doi.org/10.5194/egusphere-2024-410, 2024.

Thompson, A. M., Doddridge, B. G., Witte, J. C., Hudson, R. D., Luke, W. T., Johnson, J. E., Johnson, B. J., Oltmans, S. J., and Weller, R.: A Tropical Atlantic Paradox: Shipboard and Satellite Views of a Tropospheric Ozone Maximum and Wave-one in JanuaryFebruary 1999., Geophysical Research Letters, 27, 3317-3320, https://doi.org/10.1029/1999GL011273, 2000.

Tian, R., Ma, X., Jia, H., Yu, F., Sha, T., and Zan, Y.: Aerosol radiative effects on tropospheric photochemistry with GEOS-Chem simulations, Atmospheric Environment, 208, 82-94, https://doi.org/10.1016/j.atmosenv.2019.03.032, 2019.

Travis, K. R. and Jacob, D. J.: Systematic bias in evaluating chemical transport models with maximum daily 8 h average (MDA8) surface ozone for air quality applications: a case study with GEOS-Chem v9.02, Geoscientific Model

870   Development, 12, 3641-3648, 10.5194/gmd-12-3641-2019, 2019.

871   v. Clarmann, T., Glatthor, N., Koukouli, M. E., Stiller, G. P., Funke, B., Grabowski, U., Hopfner, M., Kellmann, S., Linden,
872   A., Milz, M., Steck, T., and Fischer, H.: MIPAS measurements of upper tropospheric C_2H_6 and O_3 during the southern
873   hemispheric biomass burning season in 2003, Atmospheric Chemistry and Physics, 7, 5861–5872,
874   https://doi.org/10.5194/acp-7-5861-2007, 2007.

875   Van Der Werf, G. R., Randerson, J. T., Giglio, L., Van Leeuwen, T. T., Chen, Y., Rogers, B. M., Mu, M., Van Marle, M. J.
876   E., Morton, D. C., Collatz, G. J., Yokelson, R. J., and Kasibhatla, P. S.: Global fire emissions estimates during 1997–
877   2016, Earth System Science Data, 9, 697-720, https://doi.org/10.5194/essd-9-697-2017, 2017.

878   Vernooij, R., Giongo, M., Borges, M. A., Costa, M. M., Barradas, A. C. S., and Van Der Werf, G. R.: Intraseasonal
879   variability of greenhouse gas emission factors from biomass burning in the Brazilian Cerrado, Biogeosciences, 18,
880   1375-1393, https://doi.org/10.5194/bg-18-1375-2021, 2021.

881   Vieira, I., Verbeeck, H., Meunier, F., Peaucelle, M., Sibret, T., Lefevre, L., Cheesman, A. W., Brown, F., Sitch, S., Mbifo,
882   J., Boeckx, P., and Bauters, M.: Global reanalysis products cannot reproduce seasonal and diurnal cycles of
883   tropospheric   ozone   in   the   Congo   Basin,   Atmospheric   Environment,   304,   119773,
884   https://doi.org/10.1016/j.atmosenv.2023.119773, 2023.

885   Vongruang, P., Wongwises, P., and Pimonsree, S.: Assessment of fire emission inventories for simulating particulate matter
886   in   Upper   Southeast   Asia   using   WRF-CMAQ,   Atmospheric   Pollution   Research,   8,   921-929,
887   https://doi.org/10.1016/j.apr.2017.03.004, 2017.

888   Wang, C., Wang, T., Wang, P., and Rakitin, V.: Comparison and Validation of TROPOMI and OMI NO2 Observations over
889   China, Atmosphere, 11, 10.3390/atmos11060636, 2020.

890   Wang, X., Fu, T. M., Zhang, L., Lu, X., Liu, X., Amnuaylojaroen, T., Latif, M. T., Ma, Y., Zhang, L., Feng, X., Zhu, L.,
891   Shen, H., and Yang, X.: Rapidly Changing Emissions Drove Substantial Surface and Tropospheric Ozone Increases
892   Over Southeast Asia, Geophysical Research Letters, 49, e2022GL100223, https://doi.org/10.1029/2022gl100223,
893   2022.

894   Weagle, C. L., Snider, G., Li, C., van Donkelaar, A., Philip, S., Bissonnette, P., Burke, J., Jackson, J., Latimer, R., Stone,
895   E., Abboud, I., Akoshile, C., Anh, N. X., Brook, J. R., Cohen, A., Dong, J., Gibson, M. D., Griffith, D., He, K. B.,
896   Holben, B. N., Kahn, R., Keller, C. A., Kim, J. S., Lagrosas, N., Lestari, P., Khian, Y. L., Liu, Y., Marais, E. A., Martins,
897   J. V., Misra, A., Muliane, U., Pratiwi, R., Quel, E. J., Salam, A., Segev, L., Tripathi, S. N., Wang, C., Zhang, Q., Brauer,
898   M., Rudich, Y., et al.: Global Sources of Fine Particulate Matter: Interpretation of $PM_{2.5}$ Chemical Composition
899   Observed by SPARTAN using a Global Chemical Transport Model, Environmental Science & Technology, 52, 11670-
900   11681, https://doi.org/10.1021/acs.est.8b01658, 2018.

901   Wells, K. C., Millet, D. B., Payne, V. H., Deventer, M. J., Bates, K. H., de Gouw, J. A., Graus, M., Warneke, C., Wisthaler,
902   A., and Fuentes, J. D.: Satellite isoprene retrievals constrain emissions and atmospheric oxidation, Nature, 585, 225-
903   233, https://doi.org/10.1038/s41586-020-2664-3, 2020.

904   Wiedinmyer, C., Akagi, S. K., Yokelson, R. J., Emmons, L. K., Al-Saadi, J. A., Orlando, J. J., and Soja, A. J.: The Fire
905   INventory from NCAR (FINN): a high resolution global model to estimate the emissions from open burning,
906   Geoscientific Model Development, 4, 625-641, https://doi.org/10.5194/gmd-4-625-2011, 2011.

907   Wiedinmyer, C., Kimura, Y., McDonald-Buller, E. C., Emmons, L. K., Buchholz, R. R., Tang, W., Seto, K., Joseph, M. B.,
908   Barsanti, K. C., Carlton, A. G., and Yokelson, R.: The Fire Inventory from NCAR version 2.5: an updated global fire
909   emissions model for climate and chemistry applications, Geoscientific Model Development, 16, 3873-3891,
910   https://doi.org/10.5194/gmd-16-3873-2023, 2023.

911   Williams, J. E., Scheele, M. P., van Velthoven, P. F. J., Cammas, J.-P., Thouret, V., Galy-Lacaux, C., and Volz-Thomas , A.:

The influence of biogenic emissions from Africa on tropical tropospheric ozone during 2006: a global modeling study, Atmospheric Chemistry and Physics, 9, 5729–5749, https://doi.org/10.5194/acp-9-5729-2009, 2009.

Williams, J. E., Scheele, M. P., van Velthoven, P. F. J., Thouret, V., Saunois, M., Reeves, C. E., and Cammas, J. P.: The influence of biomass burning and transport on tropospheric composition over the tropical Atlantic Ocean and Equatorial Africa during the West African monsoon in 2006, Atmospheric Chemistry and Physics, 10, 9797-9817, https://doi.org/10.5194/acp-10-9797-2010, 2010.

Wolfe, G. M., Nicely, J. M., St. Clair, J. M., Hanisco, T. F., Liao, J., Oman, L. D., Brune, W. B., Miller, D., Thames, A., González Abad, G., Ryerson, T. B., Thompson, C. R., Peischl, J., McKain, K., Sweeney, C., Wennberg, P. O., Kim, M., Crounse, J. D., Hall, S. R., Ullmann, K., Diskin, G., Bui, P., Chang, C., and Dean-Day, J.: Mapping hydroxyl variability throughout the global remote troposphere via synthesis of airborne and satellite formaldehyde observations, Proceedings of the National Academy of Sciences, 116, 11171-11180, 10.1073/pnas.1821661116, 2019.

Xu, R., Ye, T., Yue, X., Yang, Z., Yu, W., Zhang, Y., Bell, M. L., Morawska, L., Yu, P., Zhang, Y., Wu, Y., Liu, Y., Johnston, F., Lei, Y., Abramson, M. J., Guo, Y., and Li, S.: Global population exposure to landscape fire air pollution from 2000 to 2019, Nature, 621, 521-529, 10.1038/s41586-023-06398-6, 2023.

Xu, Z., Huang, X., Nie, W., Shen, Y., Zheng, L., Xie, Y., Wang, T., Ding, K., Liu, L., Zhou, D., Qi, X., and Ding, A.: Impact of Biomass Burning and Vertical Mixing of Residual‐Layer Aged Plumes on Ozone in the Yangtze River Delta, China: A Tethered‐Balloon Measurement and Modeling Study of a Multiday Ozone Episode, Journal of Geophysical Research: Atmospheres, 123, 11786-11803, https://doi.org/10.1029/2018jd028994, 2018.

Yang, J. and Zhao, Y.: Performance and application of air quality models on ozone simulation in China – A review, Atmospheric Environment, 293, 10.1016/j.atmosenv.2022.119446, 2023.

Yang, J., Kang, S., Hu, Y., Chen, X., and Rai, M.: Influence of South Asian Biomass Burning on Ozone and Aerosol Concentrations Over the Tibetan Plateau, Advances in Atmospheric Sciences, 39, 1184-1197, https://doi.org/10.1007/s00376-022-1197-0, 2022.

Yue, X., Hu, Y., Tian, C., Xu, R., Yu, W., and Guo, Y.: Increasing impacts of fire air pollution on public and ecosystem health, The Innovation, 5, 10.1016/j.xinn.2024.100609, 2024.

Zhang, L., Wang, X., Huang, G., and Zhang, S.: Comprehensive Assessment and Analysis of the Current Global Aerosol Optical Depth Products, Remote Sensing, 16, 10.3390/rs16081425, 2024.

Zhang, T., Wooster, M., de Jong, M., and Xu, W.: How Well Does the 'Small Fire Boost' Methodology Used within the GFED4.1s Fire Emissions Database Represent the Timing, Location and Magnitude of Agricultural Burning?, Remote Sensing, 10, 823, https://doi.org/10.3390/rs10060823, 2018.

Zhang, Y., West, J. J., Emmons, L. K., Flemming, J., Jonson, J. E., Lund, M. T., Sekiya, T., Sudo, K., Gaudel, A., Chang, K. L., Nédélec, P., and Thouret, V.: Contributions of World Regions to the Global Tropospheric Ozone Burden Change From 1980 to 2010, Geophysical Research Letters, 48, 10.1029/2020gl089184, 2021.

Zhao, T., Mao, J., Ayazpour, Z., González Abad, G., Nowlan, C. R., and Zheng, Y.: Interannual variability of summertime formaldehyde (HCHO) vertical column density and its main drivers at northern high latitudes, Atmospheric Chemistry and Physics, 24, 6105-6121, 10.5194/acp-24-6105-2024, 2024.

Zhao, T., Mao, J., Simpson, W. R., De Smedt, I., Zhu, L., Hanisco, T. F., Wolfe, G. M., St. Clair, J. M., González Abad, G., Nowlan, C. R., Barletta, B., Meinardi, S., Blake, D. R., Apel, E. C., and Hornbrook, R. S.: Source and variability of formaldehyde (HCHO) at northern high latitudes: an integrated satellite, aircraft, and model study, Atmospheric Chemistry and Physics, 22, 7163-7178, 10.5194/acp-22-7163-2022, 2022.

Zhu, L., González Abad, G., Nowlan, C. R., Chan Miller, C., Chance, K., Apel, E. C., DiGangi, J. P., Fried, A., Hanisco, T.

953 F., Hornbrook, R. S., Hu, L., Kaiser, J., Keutsch, F. N., Permar, W., St. Clair, J. M., and Wolfe, G. M.: Validation of
954 satellite formaldehyde (HCHO) retrievals using observations from 12 aircraft campaigns, Atmospheric Chemistry and
955 Physics, 20, 12329-12345, 10.5194/acp-20-12329-2020, 2020.

956